UNIVERSIDADE DO VALE DO RIO DOS SINOS - UNISINOS
UNIDADE ACADÊMICA DE PESQUISA E PÓS-GRADUAÇÃO
PROGRAMA DE PÓS-GRADUAÇÃO EM ENGENHARIA ELÉTRICA
NÍVEL MESTRADO

LUÍSE CAMBRUZZI DALLÓ

MICROFABRICATION OF ELECTRODE-INTEGRATED LIVER-ON-A-CHIP FOR IN-VITRO CELL CULTURE MONITORING

São Leopoldo
2025

LUÍSE CAMBRUZZI DALLÓ

MICROFABRICATION OF ELECTRODE-INTEGRATED LIVER-ON-A-CHIP FOR IN-VITRO CELL CULTURE MONITORING

Dissertação apresentada como requisito parcial para obtenção do título de Mestre em Engenharia Elétrica, pelo Programa de Pós-Graduação em Engenharia Elétrica da Universidade do Vale do Rio dos Sinos (UNISINOS).

Orientadora: Prof.ª Dra. Iara Janaína Fernandes

Coorientadora: Dra. Ariadna Shuck

São Leopoldo

2025

D147m Dalló, Luíse Cambruzzi.
Microfabrication of electrode-integrated liver-on-a-chip for in-vitro cell culture monitoring / Luíse Cambruzzi Dalló. – 2025.
75 f. : il. ; 30 cm.

Dissertação (mestrado) – Universidade do Vale do Rio dos Sinos, Programa de Pós-Graduação em Engenharia Elétrica, 2025.
"Orientadora: Prof.ª Dra. Iara Janaína Fernandes
Coorientadora: Dra. Ariadna Shuck".

1. Organ-on-a-chip. 2. Liver-on-a-chip. 3. Impedance spectroscopy. 4. In-vitro. I. Titulo.

CDU 621.3

Dados Internacionais de Catalogação na Publicação (CIP)
(Bibliotecária: Amanda Schuster Ditbenner – CRB 10/2517)

ACKNOWLEDGMENTS

I would like to thank my husband, Lucas, for his immeasurable support throughout this work. Your presence makes the stages of my life much lighter and happier. I thank my colleagues, especially Letícia and Vitória. This work would not have been possible without your help. To my advisors, Ariadna, Celso, and Iara, you were the light during the uncertainties of research. I thank my parents, who provided me with everything they could so I could achieve my goals. And finally, I thank myself. A thank you that may sound a little egoistic, but despite all the adversities I faced during this work and in life, I didn't give up. So, thank you to myself as well.

"Success is walking from failure to failure with no loss of enthusiasm" (CHURCHILL, Winston).

ABSTRACT

The liver is a vital organ responsible for crucial metabolic functions, drug metabolism, detoxification, and the production of proteins necessary for maintaining homeostasis in the body. However, studying liver physiology and drug metabolism has traditionally relied on animal models and two-dimensional (2D) cell cultures, which often fail to recapitulate the complex and dynamic nature accurately. Liver-on-a-chip is an emerging technology that aims to replicate the structure and functions of the human liver in a miniature and controlled in vitro platform. This study presents the fabrication and characterization of a liver-on-a-chip microfluidic device integrating microelectrodes for real-time cell culture monitoring. The device mimics the hepatic microenvironment by incorporating microchannels connected through endothelial-like capillaries, facilitating controlled nutrient exchange and waste removal under continuous perfusion conditions. The fabrication process involved three main stages: electrode fabrication, mold fabrication, and microchannel manufacturing. HepG2 cells were cultured within the microfluidic device under dynamic perfusion, demonstrating progressive adhesion, proliferation, and viability over multiple days. Impedance spectroscopy was employed to quantitatively assess cell behavior, with measurements indicating stable electrode performance and reliable monitoring of cellular dynamics. The results confirmed that the liver-on-a-chip device successfully supports long-term cell culture while providing real-time electrical characterization. This makes it a promising platform for hepatic disease modeling and pharmaceutical testing.

Keywords: organ-on-a-chip; liver-on-a-chip; impedance spectroscopy; in-vitro.

LIST OF FIGURES

LIST OF TABLES

LIST OF ABBREVIATIONS AND ACRONYMS

EIS	Electrochemical Impedance Spectroscopy
MEMS	Micro-Electro-Mechanical Systems
OoC	Organ-on-a-chip
PC	Polycarbonate
PDMS	Polydimethylsiloxane
PE	Polyethylene
PMMA	Polymethylmethacrylate
PVC	Polyvinylchloride
TEER	Transepithelial electrical resistance

GLOSSARY

1 INTRODUCTION

Clinical and pre-clinical trials are crucial in bringing new therapies to patients. However, using animals in pre-clinical tests has raised concerns from both economic and ethical perspectives, prompting the need to minimize this practice. One of the most widely recognized approaches is the 3R movement (replace, reduce, and refine). This concept was introduced in 1959 by zoologist William MS Russell and microbiologist Rex L. Burch in the book “The Principles of Human Experimental Techniques” (RUSSELL; BURCH, 1959) states that harm caused to animals in studies can be minimized without compromising the quality of scientific research (EVERITT, 2015; FONTANA et al., 2021; LANDI; SHRIVER; MUELLER, 2015).

According to the “3Rs” definition, established techniques can preserve animals from possible physical hazards. Replace: indicates that, in research with potential risk, a conscious organism must be replaced by non-conscious material, such as plants, microorganisms, etc.; to reduce, recommends that the study be carefully planned, to minimize study groups and refine, suggests that due care be taken to reduce the discomfort or suffering of the animals (CHELUVAPPA; SCOWEN; ERI, 2017).

This technology does not prevent the use of animal models in experimentation but adjusts in the sense of humanizing them. It represents the initial impulse in the scientific community and points out alternatives to the use of animals in scientific experiments. In addition to inciting a reflection on it, raising awareness of the need to conduct research and educational activities ethically (FONSECA et al., 2018). The use of cell culture is a viable alternative for the replacement of animals in research. Most preclinical cell studies today use cell monolayer experiments or Transwell technology. However, these models are static and do not represent the pathophysiology of diseases and thus do not show good transferability of findings (MOREIRA et al., 2021).

Given the above problem, an alternative is the development of an organ-on-a-chip (OoC), a technology originated from the micromanufacturing of the semiconductor industry, in which microfluidics is used to enable the study of cells and processes in a 3D environment, mimicking human physiology (ISHIDA, 2018; KIM et al., 2016).

Among organ-on-a-chip models, liver-on-a-chip models have gained significant attention and importance in hepatology and drug development for liver diseases. Traditional models such as 2D planar primary hepatocytes, hepatocyte spheroids, and hepatocyte organoids have limitations in recapitulating the liver microenvironment and

predicting drug hepatotoxicity and drug metabolism (DENG et al., 2019). Animal models also have limitations due to interspecies differences and a lack of human liver-specific metabolic activities (GHAEMMAGHAMI et al., 2012).

Liver-on-a-chip models offer several advantages that make them a preferred choice for drug development. Firstly, they can mimic the liver microenvironment and replicate the specialized roles of liver cells, such as hepatocyte metabolism and detoxification (LEE; CHO, 2016). This allows for a more accurate prediction of drug effects and toxicity. Secondly, liver-on-a-chip models can be integrated with other artificial organs on the chip to create a human-on-a-chip system, which provides a more comprehensive understanding of the overall effect of a drug (DENG et al., 2019). This is particularly important for assessing the systemic effects of drugs and their interactions with other organs.

Liver-on-a-chip models have shown promise in drug testing, particularly for assessing drug metabolism, toxicity, and efficacy on liver diseases. They have the potential to replace animal models and provide a more human-relevant in vitro liver model for preclinical drug development. The ability to control the microenvironment of liver cells in these models allows for higher throughput drug screening and the selection of drugs that are safer and more efficacious (KHETANI et al., 2015).

This work presents the design, fabrication, and characterization of a liver-on-a-chip device that integrates microfluidics and EIS for real-time, label-free monitoring of hepatic cell function. Unlike conventional approaches, this system enables continuous tracking of cell adhesion, proliferation, and barrier integrity without the need for destructive assays. A refined SU-8 photolithography process was developed to overcome fabrication challenges, ensuring highly stable microchannels and long-term culture viability. The integration of impedance spectroscopy with microscopic analysis further strengthens the interpretation of cell behavior, allowing for a correlation between electrical properties and morphological changes throughout the culture period. Additionally, this study explores the effect of electrical stimuli on hepatic cells, an underexplored aspect in liver-on-a-chip research, providing insights into cell-electrode interactions, potential bioelectronic applications, and the impact of electrical properties on liver function.

This work contributes to the advancement of microfluidic hepatic models by addressing key limitations in existing liver-on-a-chip models—such as the lack of real-time monitoring, fabrication challenges, and limited long-term culture stability. The

proposed platform offers a powerful alternative for toxicology studies, drug screening, and disease modeling, reinforcing its potential as a valuable tool for biomedical research and personalized medicine.

1.1 OBJECTIVES

1.1.1 Main Objective

This work aims to develop and prototype a microfluidic device that mimics the functioning of a human liver. This device would allow rapid testing of new products and the study of pathologies.

1.1.2 Specific Objectives

To achieve the general objective, the following specific objectives were determined:

a) Model the device, considering aspects related to geometry and usability.
b) Simulate the fluidic and electrical behavior of the device.
c) Develop manufacturing processes to produce channels and electrodes.
d) Prototype the device meeting the established criteria.
e) Perform cell culture tests.
f) Evaluate cell behavior after applying electrical stimuli, assessing the effects of electrical current on cell function.

2 LITERATURE REVIEW

2.1 THE LIVER

The liver is the largest internal organ of the human body and plays a crucial role in maintaining overall health and functioning. The liver's complex functions make it indispensable for maintaining overall health, metabolism, and proper bodily functioning (“Guyton and Hall Textbook of Medical Physiology”, [s.d.]). It performs numerous essential functions, including the following:

- Detoxification: The liver filters and detoxifies harmful substances, such as toxins, drugs, alcohol, and metabolic waste products, from the bloodstream.
- Metabolism: It regulates metabolism by processing nutrients, including carbohydrates, fats, and proteins. The liver helps convert nutrients into usable forms and produces bile to aid in the digestion and absorption of fats.
- Protein synthesis: The liver synthesizes various proteins necessary for blood clotting, immune function, and the transportation of nutrients and hormones.
- Storage: It acts as a storage site for vitamins (such as A, D, E, and K), minerals (such as iron and copper), and glycogen (a stored form of glucose).
- Detoxification of drugs and hormones: The liver breaks down and eliminates drugs, medications, and hormones from the body.
- Production of bile: The liver produces bile, a substance that helps digest and absorb fats.
- Regulation of cholesterol: It helps regulate cholesterol levels by synthesizing, storing, and removing cholesterol as needed.
- Immune function: The liver is involved in immune responses, producing immune factors and removing bacteria, viruses, and other foreign particles from the bloodstream (“Guyton and Hall Textbook of Medical Physiology”, [s.d.]).

The basic functional unit of the liver is the liver lobule, which takes the form of a cylindrical structure, measuring a few millimeters in length and ranging from 0.8 to 2

millimeters in diameter. Within the human liver, 50,000 to 100,000 individual lobules can be found (“Guyton and Hall Textbook of Medical Physiology”, [s.d.]). The hepatic sinusoid is a specialized capillary of fenestrated liver sinusoidal endothelial cells (LSECs) averaging 10 μm in diameter and 275 μm in length, as shown in Figure 1. Blood flows through the sinusoid at an average linear flow rate of 144 μm/s. Liver parenchymal tissue is composed of hepatocytes, which are large (20 to 25 μm-diameter) cuboidal epithelial cells (EHRLICH et al., 2019).

Figure 1 - Schematic of the hepatic sinusoid.

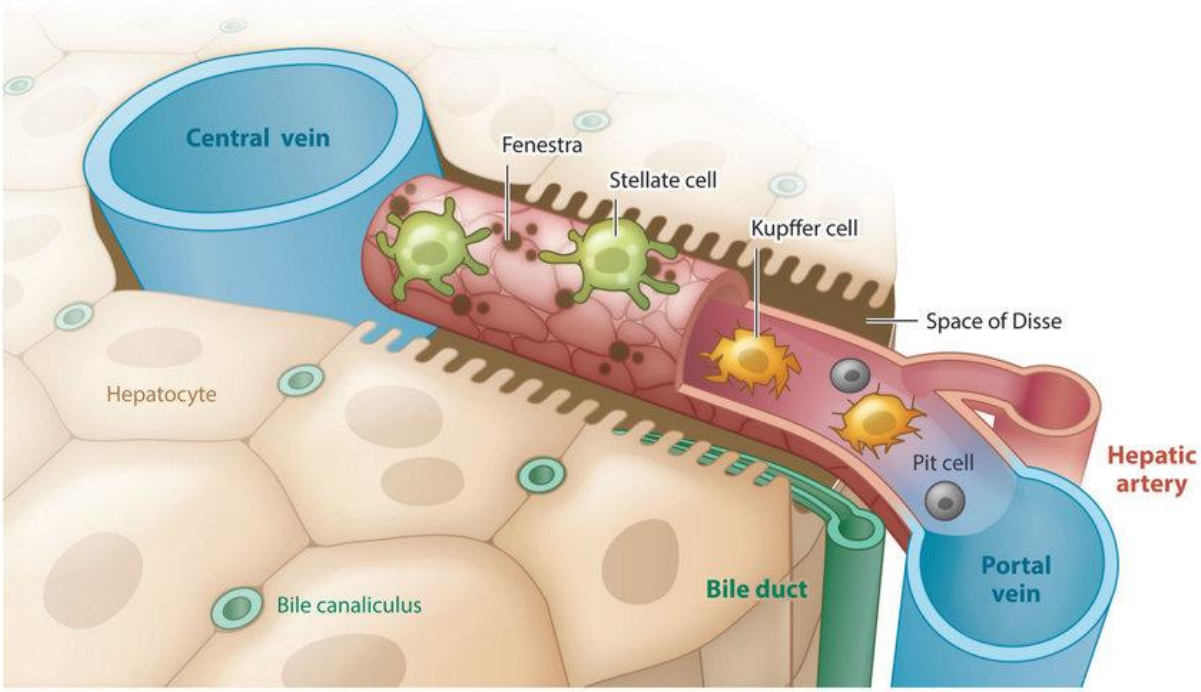

Source: Ehrlich et al. (2019).

2.2 LIVER-ON-A-CHIP

Microfluidic devices enable chemical reactions and analysis to be carried out within microchannels and microstructures, which can be produced using semiconductor microfabrication techniques like soft lithography. This technology, called lab-on-a-chip, was established as an interdisciplinary field of research combining micro and nano device technologies, chemical sensor technology, and analytical chemistry in the 1990s (KIMURA; SAKAI; FUJII, 2018).

Microfluidics is a field that utilizes microchips to miniaturize laboratory experiments, which gave rise to the concept of lab-on-a-chip. This concept gained

popularity among researchers worldwide and eventually evolved to include organ-on-a-chip applications. The latter has rapidly developed due to its potential to provide portable, cost-effective, and time-efficient biological and medical research tools. Furthermore, organs-on-a-chip offers a better mimicry of human physiology, allowing in vitro experiments with more controlled parameters of multiple human organs, as shown in Figure 2 (KIMURA; SAKAI; FUJII, 2018).

Figure 2 - Organ-on-a-chip and diseases in platforms for the modeling of human physiology and pathophysiology

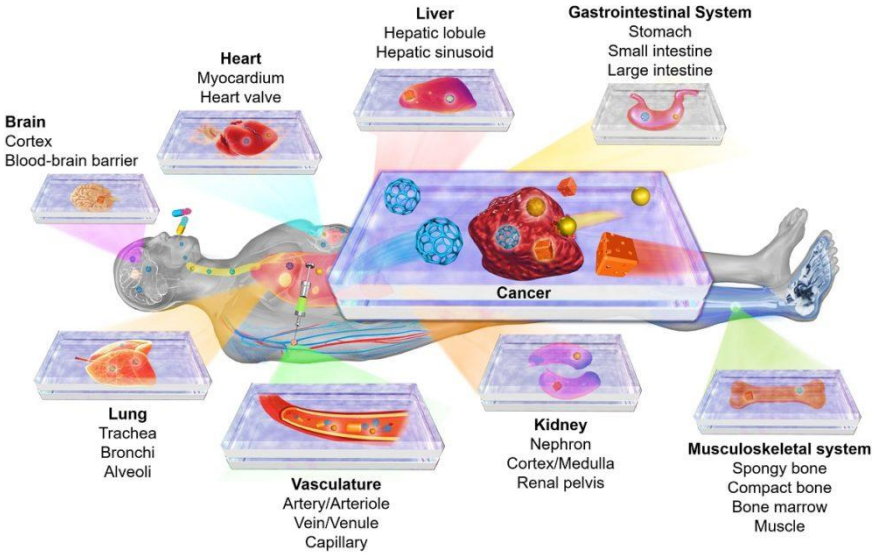

Source: (ZHANG; ZHANG; ZHANG, [s.d.]).

Liver-on-a-chip models seek to mimic the microenvironment and ultrastructure of the liver in vivo by culturing several liver cells on a chip. These models can reproduce the unique physiological functions of the liver, making them valuable tools for studying liver diseases, drug screening, and metabolic evaluation. This technology aims to replicate the structure and function of the liver on a microscale platform, allowing for more accurate and reliable in vitro studies of liver biology, disease mechanisms, and drug responses (QIU et al., 2023).

Liver-on-a-chip models are designed to replicate the flow of blood and nutrients in the liver by incorporating microfluidic channels that mimic the blood vessels. This dynamic flow system allows for the perfusion of nutrients and oxygen to the liver cells, as well as the removal of waste products, thus maintaining the viability and functionality of the cells (QIU et al., 2023).

One of the significant advantages of liver-on-a-chip technology is its potential to replace animal models in research and drug development. Animal models have limitations regarding their ability to represent human physiology and drug responses accurately. Liver-on-a-chip models provide a more physiologically relevant platform for drug testing, allowing researchers to assess the efficacy and toxicity of drugs in a more accurate and predictive manner (KHAZALI; CLARK; WELLS, 2017).

Liver-on-a-chip technology also holds promise for personalized medicine. The occurrence of liver metastases, for example, is influenced by various factors such as the primary tumor type, sex, and race. By modeling these specific settings using liver-on-a-chip platforms, researchers can develop personalized and targeted therapies for specific patient groups (KHAZALI; CLARK; WELLS, 2017). Furthermore, this technology has been extensively used in drug development and toxicity testing. The liver is a major site for drug metabolism, and liver-on-a-chip models offer a more accurate and predictive platform for evaluating the efficacy and safety of drugs. The ability to integrate drug metabolism and toxic processes in a single device is a unique advantage of liver-on-a-chip models (CONG et al., 2020).

2.3 MICROFLUIDICS

Fluids, when handled in small volumes, have different characteristics compared to larger volumes. According to Nguyen (2019, p.1)This concept can be defined as “Microfluidics is the science and engineering of systems in which the fluid behavior differs from conventional flow theory, mainly due to the small length scale of the system."

Among its particularities, the following stand out: the possibility to use minimal quantities, which is essential when an experiment has a very high cost of reagent or drug, and to carry out detections with high resolution and sensitivity; short time for analysis; and small footprints for the analytical devices. The flows in the systems are quite stable, causing fluids to flow through the channel in parallel and organized flows. These characteristics can be helpful in chemical reactions, where temperature control, reactant concentration, and reaction rate are relevant (MANZ et al., 1992; WHITESIDES, 2006).

In general, OoC allows for in vitro experiments with more controlled parameters. Significant microfluidic advances began with physics research and involved handling

very low sample volumes, typically ranging from microliters to femtoliters. For example, turbulent flow only exists at the macroscale, and laminar flow is dominant at the microscale subject to the Reynolds number. The Reynolds number is a critical dimensionless quantity in fluid mechanics used to predict flow patterns in different fluid flow situations (SOSA-HERNÁNDEZ et al., 2018).

The Reynolds number is the ratio of the internal force to the viscous force. Internal forces move the particles away from the layer, while viscous forces keep the layers moving smoothly over each other. At low Reynolds numbers, i.e., less than 500, viscous forces dominate, and flow tends to be laminar (sheet-like). A series of parallel layers can represent laminar flows without any mixing between them. However, at high Reynolds numbers higher than 2000, turbulent forces dominate, which results in differences in the velocity and direction of the fluid; thus, the flow is fully turbulent (SOSA-HERNÁNDEZ et al., 2018).

$$Re = \frac{\rho V D}{\mu} \quad (1)$$

Where:

μ - fluid dynamic viscosity in kg/(m·s);

ρ - fluid density in kg/m^3;

V - fluid velocity in m/s;

D - pipe diameter in m.

Under these conditions, there are lateral and vertical exchanges between the liquid veins that can sometimes cross each other or even move in the opposite direction to the general flow direction (eddy currents) (SOSA-HERNÁNDEZ et al., 2018).

2.4 FABRICATION TECHNOLOGIES

This section provides a comprehensive description of the fabrication technologies, encompassing a range of advanced methods and highlighting the processes that underpin the development of the liver-on-a-chip device.

2.4.1 Photolithography

Integrating microfabrication techniques, such as photolithography, into liver-on-a-chip devices has created complex three-dimensional (3D) architectures at the microscale. Photolithography allows for the precise patterning of cells and biomaterials to create high-aspect-ratio 3D structures (MAO et al., 2017).

The photolithography process is used for engraving patterns using light. This process is widely used in the electronics industry to define patterns on silicon wafers and printed circuit boards (ZAOUK; PARK; MADOU, 2006). The general process for applying the photoresist follows these steps: removal of moisture from the substrate (stove), deposition of the photoresist on the substrate (spin coating), pre-curing (heating plate), photoengraving (direct or masked), development (chemical bath with the specific developer) followed by a final cure (heating plate) (ZAOUK; PARK; MADOU, 2006). This process is exemplified in Figure 3.

Figure 3 - Process flow of photolithography and soft lithography with PDMS.

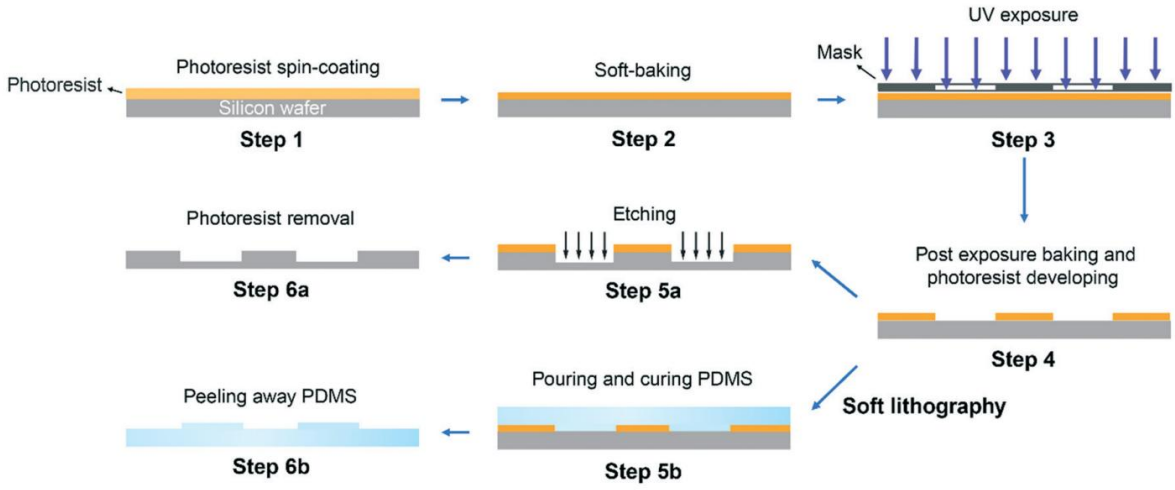

Source: Zhu et al. (2020).

As the first step in the lithography process, a thin layer of an organic polymer, a photoresist sensitive to UV radiation, is deposited on the oxide surface, as shown in Figure 4. The photoresist is dispensed onto the wafer lying on a wafer platen in a resist spinner. A vacuum chuck holds the wafer in place. A speed of about 500 rpm is commonly used during dispensing, allowing the fluid to spread over the substrate. After the dispensing step, it is common to accelerate to a relatively high speed to thin the fluid to near its final desired thickness. Typical spin speeds for this step range from

1,500 to 6,000 rpm, depending on the properties of the fluid (mostly its viscosity) and the substrate. This step can take from 10 seconds to several minutes. The combination of spin speed and time selected for this step will generally define the final film thickness. At these speeds, centrifugal force causes the solution to be low to the edges, where it builds up until it is expelled when surface tension is exceeded. The resulting polymer thickness is a function of spin speed, solution concentration, and molecular weight (measured by intrinsic viscosity) (MADOU, 2012).

The resist spinning process is of primary importance to the effectiveness of pattern transfer. The quality of the resist coating determines the density of defects transferred to the device under construction (MADOU, 2012).

Figure 4 - Resist spinner

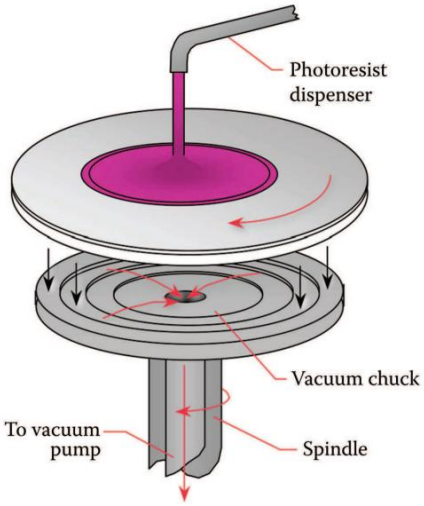

Source: Madou (2012).

After resist coating, the resist still contains up to 15% solvent and may contain built-in stresses. Therefore, the wafers are soft baked (also pre-exposure-baked or prebaked) at 90 ~ 100°C for about 20 min in a convection oven or at 75 ~ 85°C for 1~3 min with a vacuum hot plate to remove solvents and stress and to promote adhesion of the resist layer to the substrate. This is a critical step because failure to remove the solvent sufficiently will affect the resist profile. Excessive baking destroys the photoactive compound and reduces sensitivity. Thick resists may benefit from a longer bake time. The resist thickness, for both negative and positive resists, is typically reduced by 10~25% during soft baking (MADOU, 2012).

After soft baking, the resist-coated wafers are transferred to an illumination or exposure system. The purpose of the illumination is to deliver light with the proper

intensity, directionality, spectral characteristics, and uniformity across the wafer, allowing a nearly perfect transfer or printing of the mask image onto the resist in the form of a latent image. The incident light intensity (in W/cm^2) multiplied by the exposure time (in seconds) gives the incident energy (J/cm^2) or dose across the surface of the resist film. Radiation induces a chemical reaction in the exposed areas of the photoresist, altering the solubility of the resist in a solvent (MADOU, 2012).

In research laboratories, due to the need for several prototypes and tests, instead of the mask, direct recording on the photoresist (maskless lithography) is used. The equipment used for direct engraving on the photoresist is called a LaserWriter. This equipment has a light source that sensitizes the photoresist according to the pattern inserted in the equipment's software. The substrate is positioned on a mobile table that moves according to the inserted design. This process allows the fabrication of structures with dimensions smaller than 1 μm (MADOU, 2012).

After exposure, the unexposed part of the photoresist (in the case of negative type photoresist) is solubilized by a specific chemical solution for developing the photoresist, or developer. Development is the dissolution of unpolymerized resist that transforms the latent resist image formed during exposure into a relief image that will serve as a mask for further subtractive and additive steps (ZAOUK; PARK; MADOU, 2006).

2.4.2 Sputtering

The physical deposition of materials is fundamental for the fabrication of microdevices. Two techniques allow the physical deposition of metals and dielectrics to be carried out: Physical Vapor Deposition (PVD) or cathodic vapor deposition or sputtering. The advantages of sputtering are the possibility of depositing any type of material, be it conductive or dielectric, precision in thickness control, and repeatability of the deposition (MATTOX, 2002).

The sputtering process uses targeted ion bombardment to remove atoms from a selected target. Initially, a vacuum is generated inside the chamber. An inert gas is injected at low pressure (usually Argon), which, in turn, is ionized and accelerated toward the target by the electric field created by a high-voltage source. The collision of the ionized gas atoms with the target removes the material in the target, creating a

vapor of removed material deposited on the surface of interest (substrate) (ABDELRAHMAN, 2015).

The deposited layer's thickness depends on controllable parameters, such as power, process time, pressure, and distance from the target. Some additional parameters may also interfere with the characteristics of the deposited material (BUNSHAH; DESHPANDEY; DESHPANDEY, 1985).

2.5 MATERIALS

This section covers the diverse array of materials utilized in the fabrication process of the liver-on-a-chip device.

2.5.1 Silicon (Si)

The vast variety of microfabrication processes for microfluidic devices and MEMS (Micro-Electro-Mechanical Systems) is mainly inherited from the microelectronics industry, where silicon is the most prevalent material. Silicon is fundamentally necessary for microelectronics because of its semiconductor properties. The silicon wafers are formed by a single crystal and present a diamond-like cubic network, depicted in Figure 5. The primitive cell is formed by a face-centered cubic structure with four more atoms placed in the interstices of the structure, and these atoms are distributed two in each one of the plans (LEE; SUNDARARAJAN, [s.d.]).

Figure 5 - Silicon crystallographic structure.

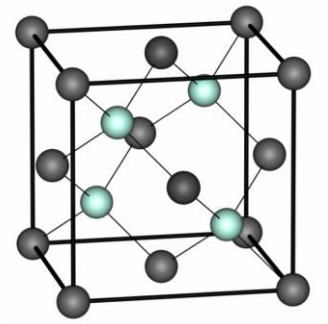

Source: Theses; Weerasinghe (2006).

2.5.2 Platinum

Various materials, including gold (Au), palladium (Pd), graphite, and platinum (Pt), are commonly used for electrode fabrication in biosensors. However, among these materials, Pt is more stable and inert compared to the other materials and shows a better sensitivity in most applications (O'NEILL et al., 2004; THUY; TSENG, 2016).

Furthermore, it is known that Pt shows better results for biocompatibility compared to Au. This means that Pt is more compatible with biological systems and less likely to induce adverse reactions when used in biosensors (LI et al., 2014).

2.5.3 Photoresist

Photoresists are light-sensitive materials composed of a polymer, a sensitizer, and a solvent. The polymer changes its structure when exposed to radiation. The solvent allows the photoresist to flow and form thin layers on the surface of the substrate or wafer. Finally, the sensitizer, or inhibitor, controls the photochemical reaction in the polymer phase (QUERO; PERDIGONES; ARACIL, 2018).

Photoresists can be classified as positive or negative. In positive photoresists, the photochemical reaction during exposure weakens the polymer, making it more soluble for the developer to achieve the positive pattern. The mask, therefore, contains an exact copy of the pattern, which must remain on the substrate or wafer, as a stencil for further processing. In the case of a negative photoresist, exposure to light causes the photoresist to polymerize, so the photoresist remains on the surface of the substrate where it is exposed, and the developer solution removes only the unexposed areas. Therefore, the masks used for negative photoresists contain the pattern's photographic inverse or "negative" to be transferred. Figure 6 shows the result of exposing both photoresists. As can be seen, the same mask produces complementary structures (QUERO; PERDIGONES; ARACIL, 2018). The advantages of negative photoresists are good adhesion to silicon, lower cost, and shorter processing time. The benefits of positive photoresists are better resolution and thermal stability (QUERO; PERDIGONES; ARACIL, 2018).

Figure 6 - Positive and negative resist: exposure, development, and pattern transfer. (a) Negative resists remain in the exposed region. (b) Positive resists develop in the exposed region.

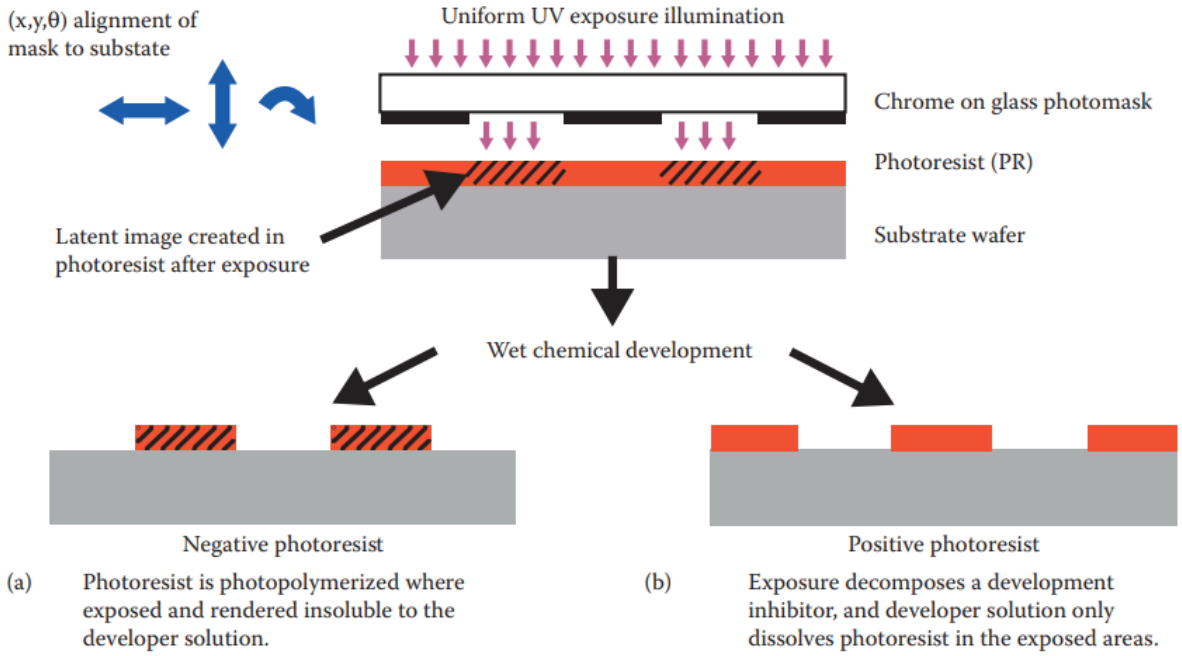

Source: Madou (2012).

2.5.4 Polydimethylsiloxane (PDMS)

Due to the diversity of MEMS applications and commercialization, it was necessary to find processes and materials that allow mass production and simultaneous cost reduction. Likewise, the increasing number of BioMEMS applications has led to a departure from traditional silicon-based processing and a search for different materials. New fabrication techniques, such as soft lithography, have stimulated the use of biocompatible materials, such as polymers (XIA; WHITESIDES, 1998). The practicality of polymers for manufacturing with rapid prototyping and mass production techniques, as well as the lower cost compared to silicon and glass, make these materials particularly attractive for the development of BioMEMS (DENG et al., 2000; MATA; FLEISCHMAN; ROY, 2005a).

Polycarbonate (PC), polymethylmethacrylate (PMMA), polyvinylchloride (PVC), polyethylene (PE), and polydimethylsiloxane (PDMS) are some of the polymer candidates for low-cost mass production of BioMEMS devices (DESPA; KELLY; COLLIER, [s.d.]; DUFFY et al., 1998; LEE et al., 2001).

In this context, PDMS is a silicone elastomer widely used to develop MEMS and microfluidic components involving biomedical applications. This silicone is a mixture of linear polymers of totally methylated siloxane, constituted by units of formula $(CH_3)_2SiO$, stabilized by terminal units of formula $(CH_3)_3SiO$, represented in Figure 7. It is chemically inert, thermally stable, permeable to gases, simple to handle and manipulate, exhibits isotropic and homogeneous properties, and less costly than silicon. It can also conform to submicrometric resources for the development of microstructures (JO et al., 2000; MATA; FLEISCHMAN; ROY, 2005b; MCDONALD; WHITESIDES, 2002; UNGER et al., 2000; XIA; WHITESIDES, 1998)

Figure 7 - Chemical structure of polydimethylsiloxane.

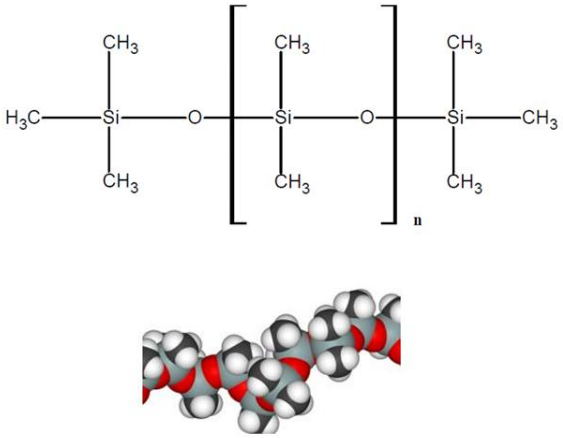

Source: Renata; Moreira (2013).

The use of PDMS for BioMEMS applications was driven by an additional factor: the development of soft lithography techniques such as microcontact printing, replica molding, micro-transfer molding, capillary micromolding, and solvent-assisted micromolding (XIA; WHITESIDES, 1998). These techniques generally require using PDMS to create an elastomeric mold that embeds microstructures for transferring physical patterns onto a subsequent substrate. Furthermore, PDMS is transparent, non-fluorescent, biocompatible, and non-toxic and has traditionally been used as a biomaterial in catheters, drainage tubes, pacemaker insulation, membrane oxygenators, and ear and nose implants. Table 1 shows the properties of this material (MATA; FLEISCHMAN; ROY, 2005a).

Table 1 - PDMS properties

Property	PDMS Sylgard 184®
Appearance	Transparent
Viscosity (mPa·s)	3,900
Modulus of elasticity (MPa)	1.8
Thermal expansion coefficient (μm/mK)	310
Thermal conductivity (W/mK)	0.18
Dielectric constant (ε_0)	2.65
Resistivity (Ω·cm)	$1.2x10^{14}$

Source: SCHNEIDER (2008).

As already mentioned, PDMS is supplied in a kit consisting of two liquid reagents, one of which is the base and the other the hardener. After mixing these two components, it is verified that the PDMS in the liquid state changes to the rubber state. The main base constituent is dimethyl vinyl, terminated by dimethylsiloxane. On the other hand, the curing agent is produced based on siloxane and methyl-dimethyl. In the presence of a platinum catalyst, a hydrosilation reaction takes place that links the siloxane units with the terminal vinyl groups of the base polymers, thus transforming the short chains of the liquid polymer into an elastomeric network (RENATA; MOREIRA, 2013).

2.6 ELECTROCHEMICAL IMPEDANCE SPECTROSCOPY

Electrochemical impedance spectroscopy (EIS) plays a crucial role in cell culture by providing valuable information about cell processes, barrier function, and tissue differentiation. It is a non-invasive technique that allows real-time monitoring of cell cultures and provides insights into various aspects of cell behavior and function (KAVAND et al., 2022; WACOGNE et al., 2022).

One of the main functions of EIS in cell culture is the measurement of transepithelial electrical resistance (TEER). TEER is a widely accepted technique for assessing the integrity of tight junction dynamics in cell culture models of endothelial and epithelial monolayers. It serves as an indicator of the integrity of cellular barriers before evaluating their transport properties. TEER measurements can be performed in

real-time without causing cell damage and are based on measuring ohmic resistance or impedance across a broad spectrum of frequencies (SRINIVASAN et al., 2015).

EIS also studies cell processes such as attachment, morphology, motility, and barrier function. It provides valuable information about the behavior and characteristics of cells in different culturing conditions, including suspended, 2D, or 3D cultures (KAVAND et al., 2022). By analyzing impedance spectra, researchers can gain insights into cell concentration, viability, and distribution (DE LEÓN; PUPOVAC; MCARTHUR, 2020; VACCARI et al., 2021)

In organ-on-chip technology, EIS is also employed to assess transepithelial barrier function and tissue structure. By combining EIS with electrical stimulation, researchers can gain insights into the barrier function and tissue differentiation of organ-on-chip models (VAN DER HELM et al., 2019).

3 METHODOLOGY

This chapter describes the methodology for device fabrication and cell culture. The required equipment and materials are detailed, along with the test procedures that will be adopted. The flowchart shown in Figure 8 describes the steps that will be carried out. The equipment models used herein are listed in Table 2.

Figure 8 - Process Flowchart.

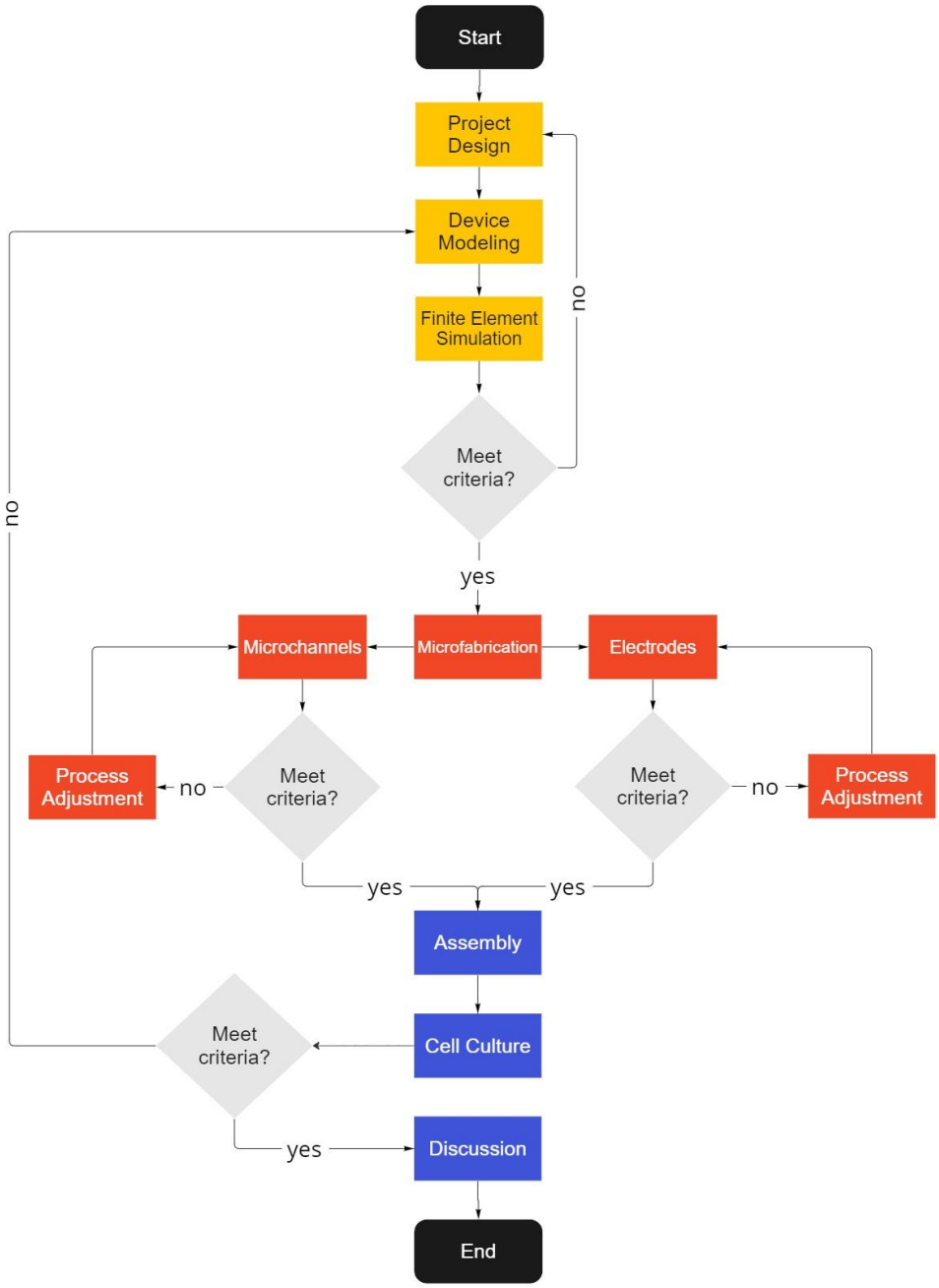

Source: Author.

Table 2 - Equipment models.

Equipment	Model
Vacuum Pump	TE-0581 (Tecnal)
Hot Plate	HP-200 (Sawatec)
Oven	400 ND (Ethik Technology)
Metallographic Microscope	Axio Lab.A1 (Zeiss)
Stereo Microscope	S9i (Leica)
Microwriter	ML3 (Durham Magneto Optics Ltd.)
Plasma	PE-200 (Plasma Etch)
Plasma	PlasmaPro®100 Cobra (Oxford)
Spin Coater	SM-200 (Sawatec)
Spin Coater	Spin 3000 (Laurell)
Sputtering	AC450 (Alliance Concept)

Source: Author.

3.1 DESIGN

Unlike the traditional OoC fabrication model using membranes in a vertical orientation, this device was designed in a planar orientation. This configuration was chosen due to the ease of fabrication, perfusion of the cell nutrient, and microscope view (CHAN et al., 2014; LEE; JUN, 2019; RAMADAN; ZOUROB, 2020).

The device was modeled on SolidWorks, and it's based on the liver-on-a-chip design proposed by GORI (2016). It is designed with an endothelial-like perfusion barrier connecting the nutrient channel and culture chamber. Thus, cells of different types can be cultured near each other, enabling them to be fluidically and chemically connected but physically isolated, to reproduce the typical human liver micro-unit, the hepatic sinusoid. This micro-unit comprises a cluster of hepatocytes surrounded by highly fenestrated and permeable endothelial cells. It is represented by a grid of closely spaced and parallel microchannels designed to mimic an endothelial-like barrier and replicate the characteristics of tissue microvasculature.

3.2 FINITE ELEMENT SIMULATION

Finite element simulations for liquid flow and electric field are performed using COMSOL Multiphysics 6.0 (Comsol Inc., Burlington, MA, USA). The stationary incompressible Navier-Stokes equations are used by this application's Partial

Differential Equation (PDE) model. Equation 2 is the balance of momentum from Newton's second law. Equation 3 is the equation of continuity, where zero on the right-hand side states that fluid is incompressible. Therefore, the flow pattern depends only on the Reynolds number (NGUYEN; HOANG, 2017).

$$\rho \cdot (u \cdot \nabla)u = \nabla \cdot [-p + K] + F \quad (2)$$

$$\rho \cdot \nabla \cdot u = 0 \quad (3)$$

Where:

ρ = Density of the fluid in kg/m^3.

∇p = Pressure gradient in N/m^3.

u = Velocity field in m/s.

K = Viscous stress tensor in N/m^2.

F = Body forces in N/m^3.

Several equations are used to simulate the electric field generated by two platinum electrodes in PDMS. The effect of the electric field in materials, where the current density is proportional to the electric field, is described by the constitutional equation known as Ohm's law, Equation 4 ("AC/DC Module User's Guide", 2018).

$$J = \sigma \cdot E \quad (4)$$

Where:

J = Current density in A/m^2.

E = Electric field intensity in V/m.

σ = Electric conductivity in S/m.

A generalized form of constitutive relationships is useful for nonlinear materials, such as PDMS. The relation defining the current density is generalized by introducing an exterior current source, J_e. The resulting constitutive relation is represented in Equation 5.

$$J = \sigma \cdot E + J_e \quad (5)$$

The Layer Current Source is available for both boundaries and edges. A boundary represents a volumetric source of current Qj,v inside the selected layers (SI unit: A/m3), as shown in Equation 6.

$$\nabla \cdot J = Q_{j,v} \tag{6}$$

The equation for the electric potential applied on the electrodes is described in Equation 7.

$$E = -\nabla \cdot V \tag{7}$$

Where:

E = Electric field in V/m.

V = Electric scalar potential in V.

For the simulation, the following materials were selected: PDMS (microchannels), water (culture media), platinum (electrodes), glass (support base), and human myocardium (cells). Table 3 shows the simulation model parameters.

Table 3 - Model Parameters.

Model Parameters	**Values**
PDMS conductivity (σ)	1.5 S/m
PDMS relative permittivity (εr)	80.1
Initial Voltage	0 V
Applied Voltage	0.3 V
Flow Velocity	1 µm/s
Temperature reference	293.15 K

Source: Author.

3.3 DEVICE FABRICATION

The device is manufactured using the following steps, which will be described in this chapter: electrode fabrication, mold fabrication, and microchannel fabrication.

3.3.1 Electrodes Fabrication

Electric measurements are conventionally obtained using electrodes in parallel so that the electrical current flows across the cell barrier (HILDEBRANDT et al., 2010; LEE et al., 2006). In this approach, there are two electrodes placed at the bottom of the microchannel, and the current flows from one electrode to another, crossing the cell barrier twice (YESTE et al., 2018). Figure 9 shows the fabrication steps.

Figure 9 - Electrodes fabrication process.

Source: Author.

Using a glass slide, 0.8 µm of the photoresist KL5310 is deposited using a spin coater at rotation 2000 rpm for 50 s, Figure 9 (a). This layer defines the design of the electrodes as a mask. Afterward, a pre-cure step was performed in the hot plate at 90 °C for 60 s. The geometry exposure was performed in MicroWriter with a 90 mJ/cm^2 dose and 1 µm lens. The post-bake was carried out at 115 ºC for 60 s, and then the photoresist was developed with manual agitation using AZ 326 (Merck) for 20 s, Figure 9 (b). The dimensions were evaluated in the metallographic microscope, and after the glass slide was submitted to 150 ºC for 5 min in a hotplate for the hardbake step.

Figure 9 (c) shows the titanium (Ti) and Pt deposition performed using sputtering. Ti was deposited to improve the adhesion of Pt in the glass slide. For this step, the used parameters are 150 W for 10 min for each metal. To conclude the

electrode fabrication, the slide was submerged in KL Remover (Kem Lab) at 60 °C for 30 min to remove the unwanted deposition areas using a lift-off technique.

3.3.2 Mold Fabrication

A mold is fabricated to define the structures in PDMS. The process flowchart is shown in Figure 10.

Figure 10 - Mold fabrication flowchart.

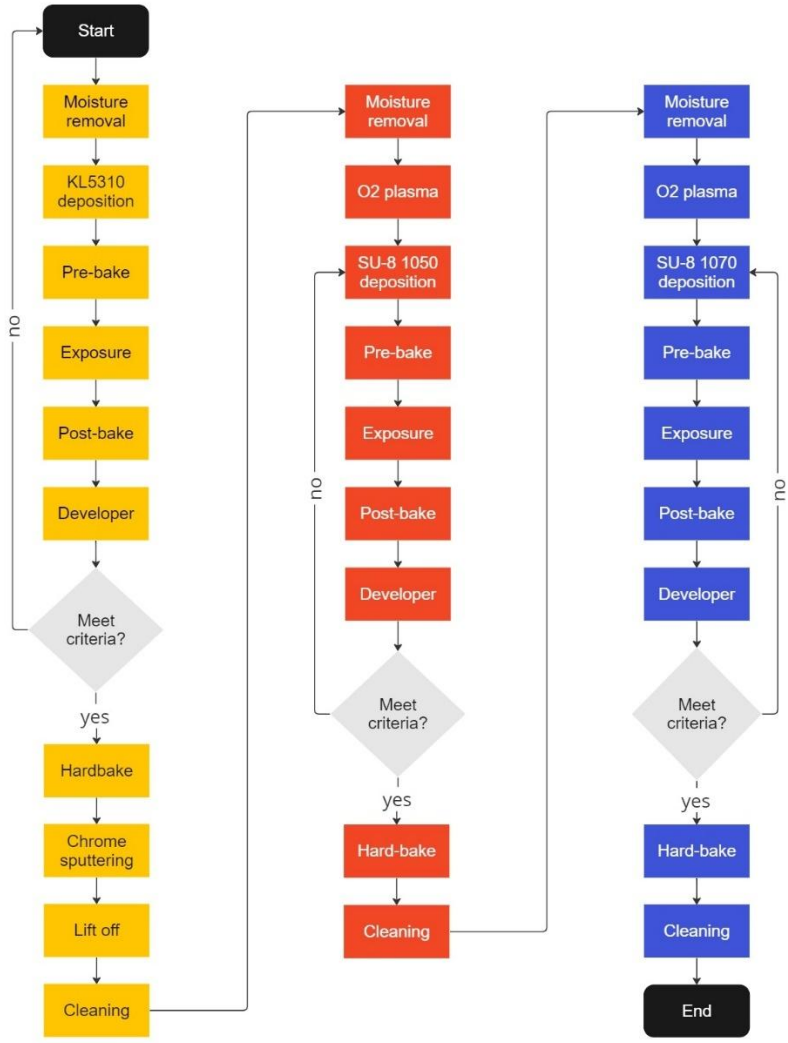

Source: Author.

As two lithograph processes overlap, alignment marks are necessary, as shown in Figure 11. For this, a silicon wafer is placed in an oven at 150 °C for 30 min to remove moisture. Afterward, oxygen plasma is performed for 5 min at 150 W to clean and improve the photoresist's adhesion.

After the wafer returns to room temperature, 0.8 µm of the KL 5310 photoresist is deposited using a spin coater at a speed of 2000 rpm for 45 s, Figure 11 (a). The wafer is pre-baked at 90 °C for 60 s.

To define the geometry of the alignment marks, the photoresist is exposed using a MicroWriter at 90 mJ/cm^2 and a 1 µm lens. The post-bake is conducted at 115 °C for 60 s, and the photoresist can then be developed. Revelation is performed for 20 seconds using AZ 326 (Merck) and the hardbake at 150 ºC for 5 min, Figure 11 (b).

After 150 nm of Chrome (Cr) is deposited on sputtering at 150 W for 12 min, Figure 11 (c), and the unwanted areas are removed using AZ 100 Remover (Merck) at 60 °C for 30 min, Figure 11 (d). The wafer is then submitted to the oven at 150 °C for 1 h to remove moisture.

Figure 11 - Alignment mark fabrication process.

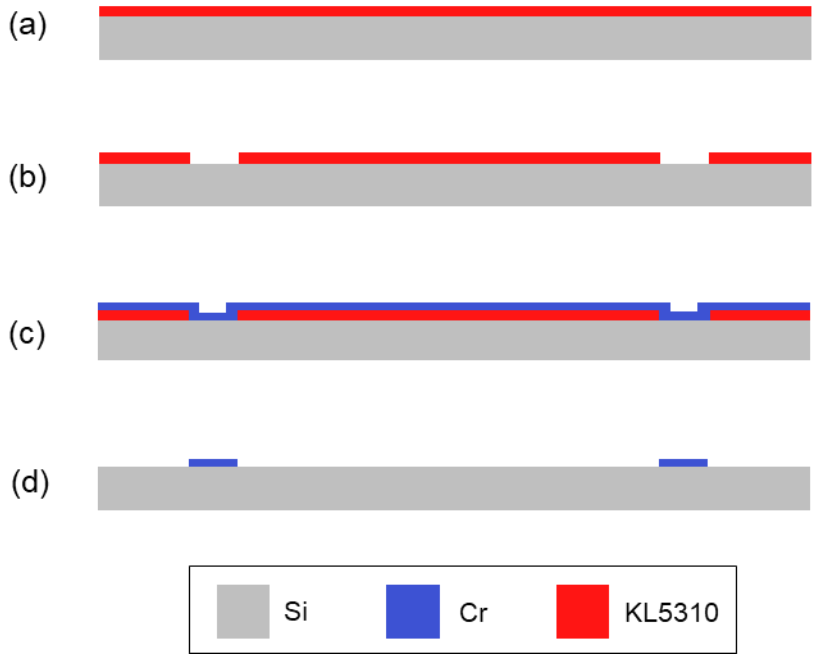

Source: Author.

The following steps are the deposition of different SU-8 to fabricate the various thicknesses of the capillaries and microchannels, presented in Figure 12. To produce the capillaries, 5 µm of SU-8 1050 is deposited in a spin coater at the rotation 1660 rpm for 40 s, Figure 12 (b). Subsequently, the pre-bake is carried out at 120 ºC for 60 s following exposure in MicroWriter with 2500 mJ/cm^2 dose and 1 µm lens, Figure 12 (c). The post-bake is realized at 65 °C for 1 min and 95ºC for 5 min. SU-8 is developed

using EBR with manual agitation for 20 s followed by isopropanol cleaning, Figure 12 (d).

Subsequently, the microchannels step is performed. For this, the wafer is submitted to the oven at 150 °C for 1 h to remove moisture. The SU-8 1070 is deposited in a spin coater at 650 rpm rotation for 40 s, Figure 12 (e). As this SU-8 has a higher viscosity than other commonly used photoresists, a relaxation time of 1 h is necessary to guarantee the planarity of the deposition. Afterward, the wafer can be submitted to the hotplate for 30 min at 65 ºC followed by 4 h at 95 ºC. The exposure is performed with a 5500 mJ/cm^2 dose using a 1 µm lens, Figure 12 (f). The post-bake is carried out for 15 min at 65 ºC and 40 min at 95 ºC following the developing step using EBR for 12 min using manual agitation, Figure 12 (g). After microscope evaluation, the mold is submitted to 150°C for 4 h for the hard baking. The thickness of the photoresist deposition will be evaluated using optical profilometry.

Figure 12 - Mold fabrication process.

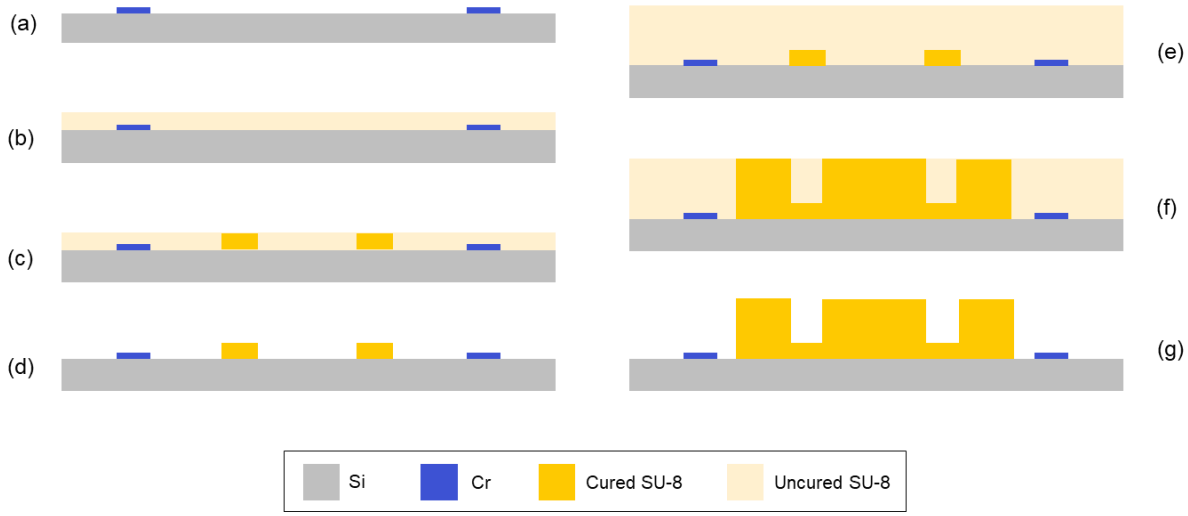

Source: Author.

3.3.3 Microchannels Fabrication and Assembly

Using the produced mold, the microchannels are fabricated, as shown in Figure 13. The PDMS was mixed with the curing agent in a 10:1 ratio and deposited on the mold, Figure 13 (b). Afterward, a vacuum is necessary to remove bubbles, and the PDMS is cured for 1 h at 80°C Figure 13 (c).

Figure 13 - Microchannels fabrication process.

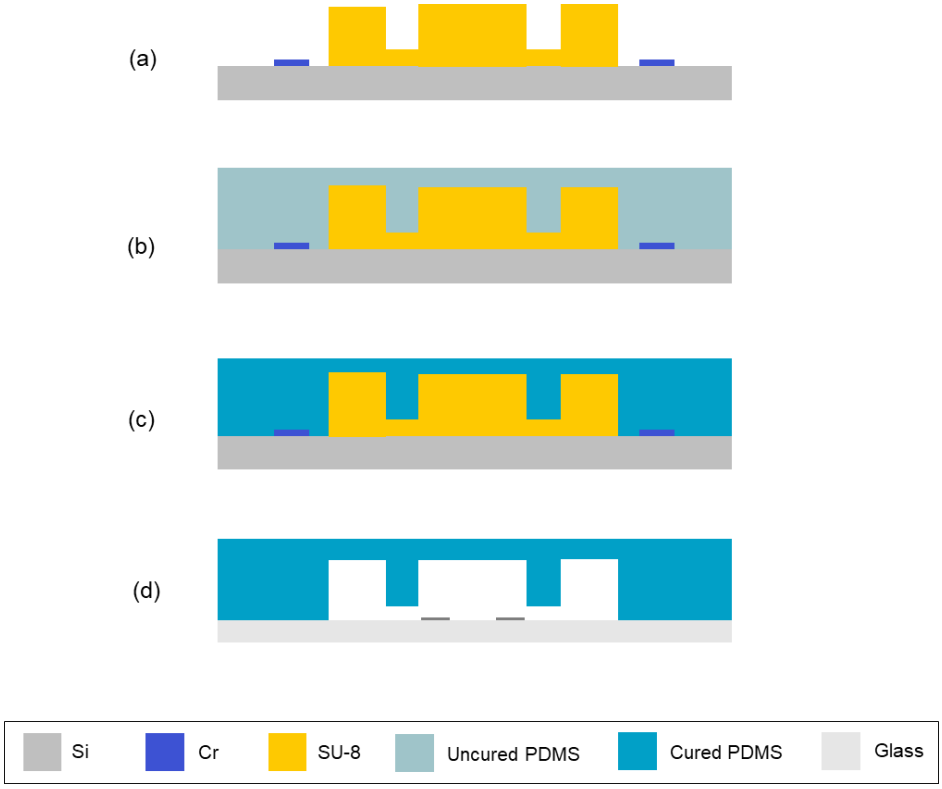

Source: Author.

For assembly of the PDMS microchannels in the electrodes fabricated, the channels undergo a cleaning process in acetone for 5 min and are rinsed with ultrapure water. Afterward, they are immersed in isopropyl alcohol for another 5 min and rinsed again. The canals are then dried in nitrogen flow and at ambient temperature. The PDMS microchannels and electrodes are submitted to O_2 plasma at 150 W for 5 min and attached with manual pressure using a stereo microscope for alignment Figure 13 (d). To guarantee adhesion, the device is submitted to 80°C overnight.

3.4 CELL CULTURE

The cells used were HepG2 cells, provided by the Stem Cell Research Institute of the Federal University of Rio Grande do Sul. The cells are stored in culture bottles with DMEM-High medium (Gibco® DMEM, powder, Low Glucose) prepared according to the manufacturer's instructions and supplemented with 10% fetal bovine serum (Gibco® Fetal Bovine Serum) and 1% antibiotic (Gibco® Penicillin Streptomycin) and maintained in an incubator for cultivation at 37 ºC with 5% CO_2. The culture medium will be changed every 2 days, and at least two cell passages will be performed before

starting the experiments. Each chip uses 10^6 cells. The cell culture tests will be conducted at the itt Nutrifor (UNISINOS).

Figure 14 - Cell culture.

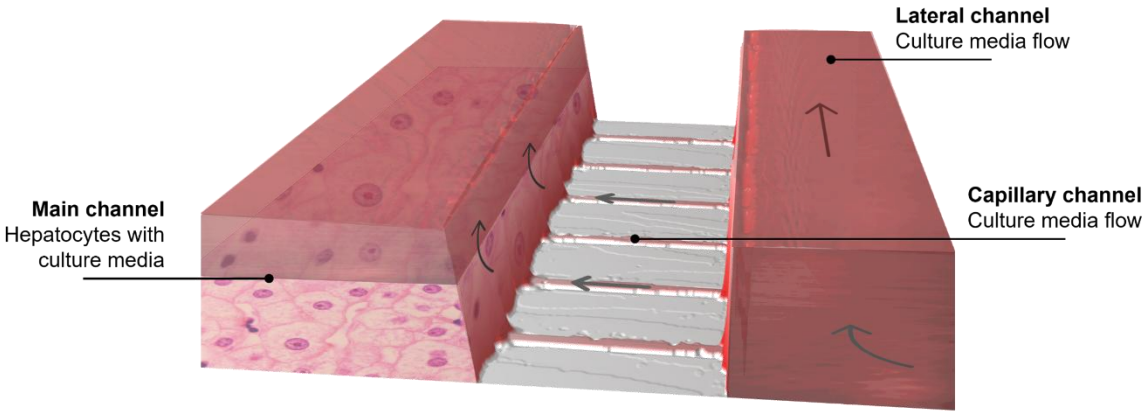

Source: Author.

The cells were cultured using microfluidic perfusion, employing a network of parallel microchannels that emulate the endothelial barrier found in a liver sinusoid, shown in Figure 14. This setup enables a continuous exchange of nutrients and waste removal, resembling natural physiological conditions.

3.4.1 Impedance Spectroscopy

To assess cellular behavior quantitatively, impedance spectroscopy was employed on the liver-on-a-chip device. The first step involves validating the electrodes using Palmsens4 (Palmsens) to ensure repeatability with ultrapure water. Subsequently, the tests will be conducted at various stages of maturation and cell death, monitoring cell viability and culture stability with the results compared to optical evaluations. Following these tests, the device will be capable of measuring parameters such as steatosis or drug resistance without causing any harm to the cell culture.

4 RESULTS AND DISCUSSION

The following sections present the design, fabrication, and characterization of the liver-on-a-chip device and the analysis of impedance spectroscopy measurements and microscopic observations to evaluate cell behavior over time.

4.1 DESIGN

The design was modeled in SolidWorks and contains a main microchannel (blue) and a perfusion microchannel (red). The channels are connected by capillaries, forming an endothelial-like barrier that allows communication and perfusion between them, as shown in Figure 15.

Figure 15 - Device modeling.

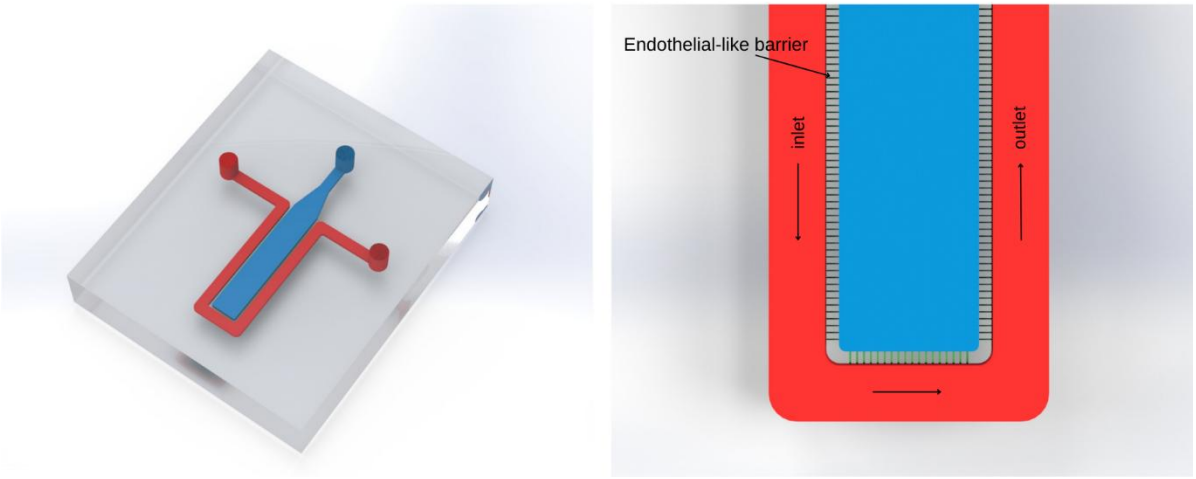

Source: Author.

4.2 FINITE ELEMENT SIMULATION

The behavior of the fluid, especially the velocity profile, directly influences the distribution of nutrients, oxygen, and chemical compounds to the cells cultured within the chip. The fluid dynamics and the electric behavior were simulated using COMSOL Multiphysics. Figure 16 shows the result of the fluid dynamics simulation.

The different colors seen in the legends represent the difference in velocity according to the position of the microchannel. The average velocity is increasingly

reduced when laminar flow is near the wall. The maximum velocity occurs at the centerline of the microchannel. This pointed out that the fluid elements in the center will move at a higher speed than those closer to the wall. This behavior mimics the physiological conditions of blood flow in the microvasculature, ensuring that cells experience appropriate shear forces (KIM et al., 2013; TSVIRKUN et al., 2017).

Figure 16 - (a, b) Velocity magnitude and (c) Electrical Field simulation.

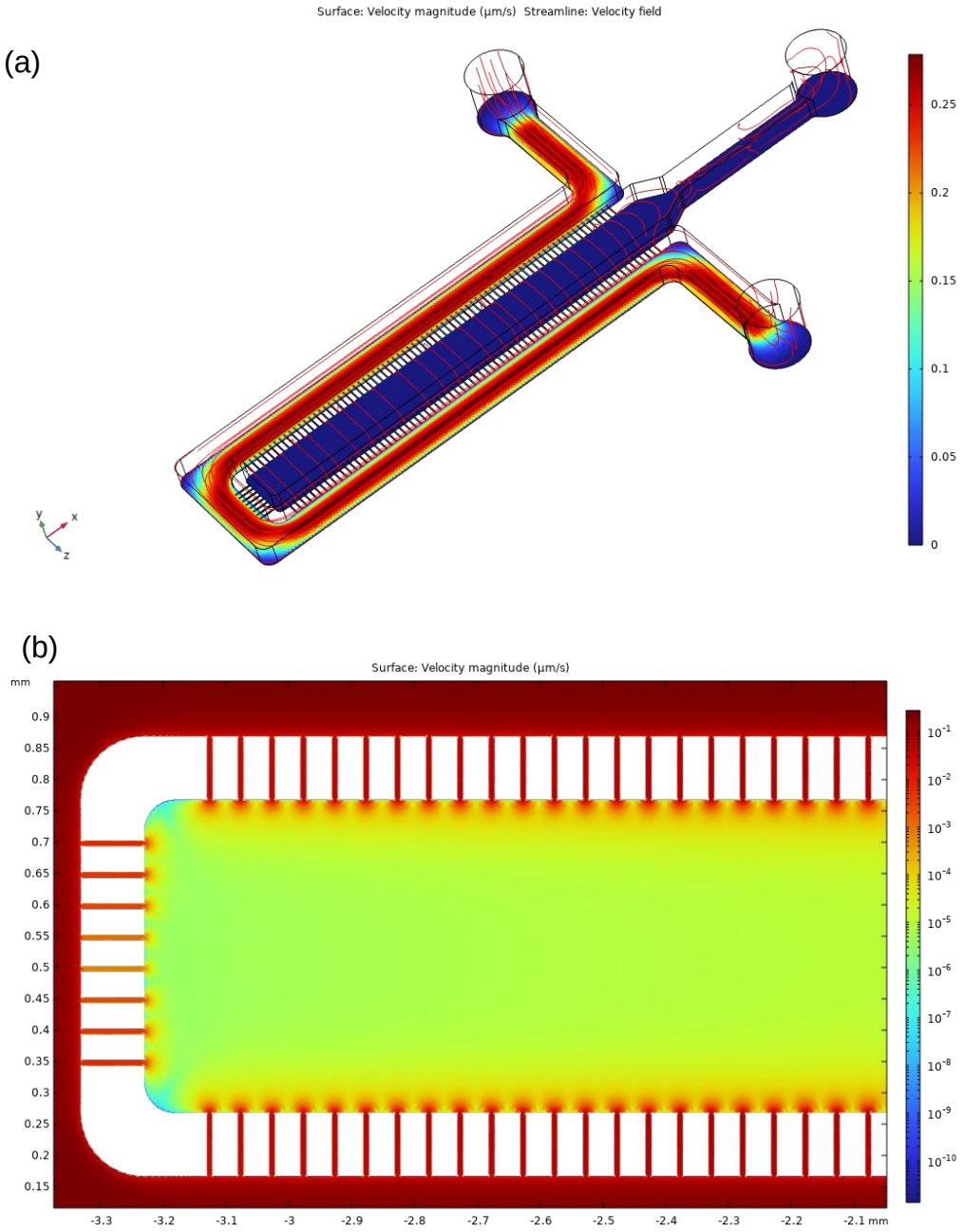

(c)

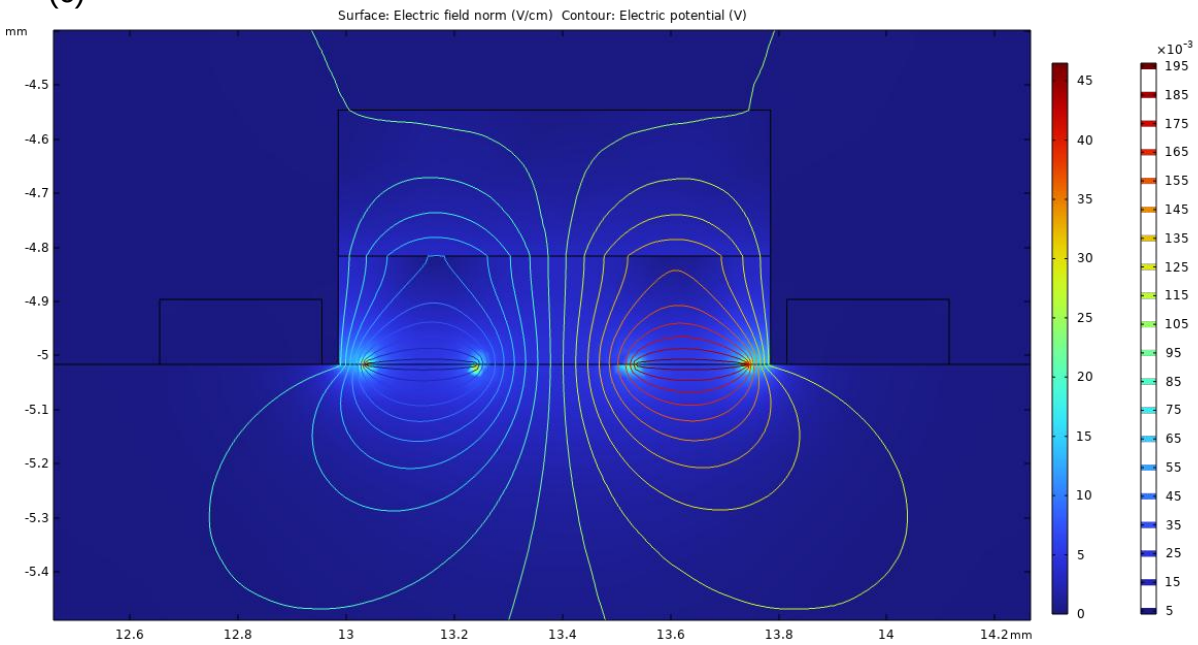

Source: Author.

The electric simulation is shown in Figure 16 (c). The simulation presented in the liver-on-a-chip model aims to analyze the distribution of the electric field generated to measure the impedance of the cells cultured on the chip. The electric field lines, represented by the colors in the image, indicate areas of high and low field intensity, which are crucial for understanding how the electric current interacts with the cells. The electrical impedance, which varies according to the cells' properties such as conductivity and membrane characteristics, is a key parameter for monitoring cell health and cell-cell interactions (TANDON et al., 2011; VISONE et al., 2018).

4.3 DEVICE FABRICATION

This chapter provides a comprehensive overview of the liver-on-a-chip fabrication process. The device's fabrication is divided into the following stages: mold fabrication, microchannel manufacturing, and assembly.

4.3.1 Electrode Fabrication

The microfabrication process of the electrodes on a glass slide was successfully executed following the planned methodology. The initial patterning of the electrodes using the photoresist KL5310 resulted in well-defined designs, as confirmed through

visual inspection under a metallographic microscope. The sputtering deposition of titanium (Ti) and platinum (Pt) was achieved with consistent layer thickness and strong adhesion to the glass substrate.

Figure 17 - Fabricated electrodes.

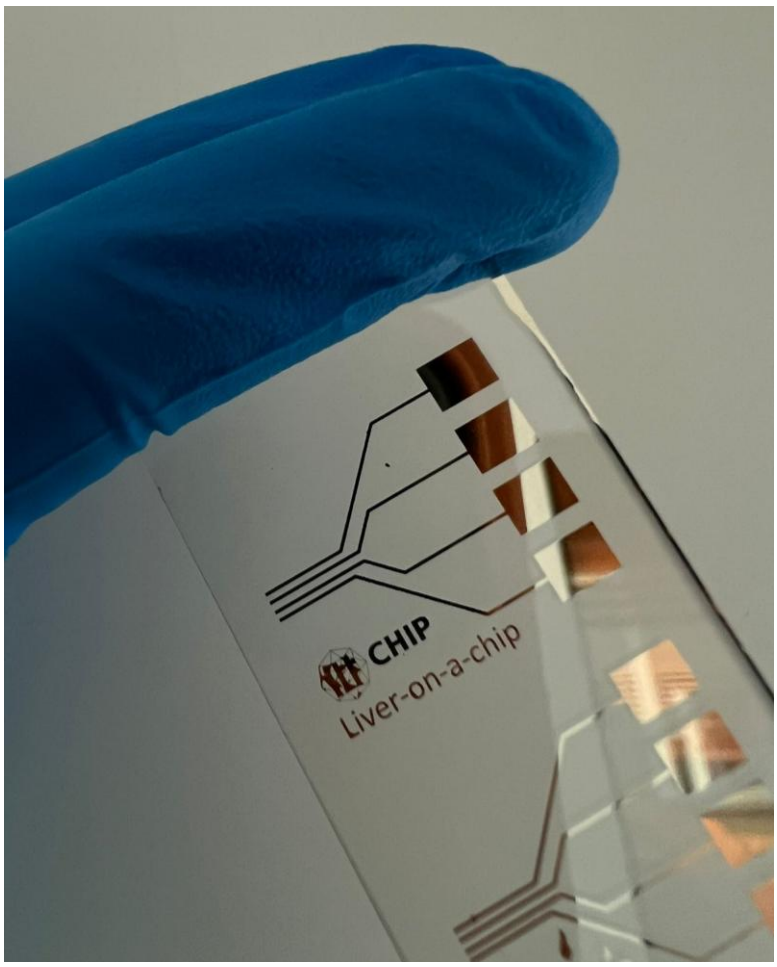

Source: Author.

4.3.2 Mold Fabrication

4.3.2.1 Mold Version 1

The fabrication of the capillaries, which enables communication between the microchannels, faced a problem: the detachment and deformation of the capillaries after the development step. To solve this problem, the process of this SU-8 was changed. The first change was not to apply isopropanol with a wash bottle directly onto the wafer, as this force could be causing capillary drag. Isopropanol was placed in a Petri dish, and the wafer was dipped. The second change was not to dry the wafer

using nitrogen, letting it dry naturally. With these two alterations, the capillaries didn’t present the detachment, and the fabrication was performed successfully. The result of this process is shown in Figure 18.

Figure 18 - Microchannels photolithography.

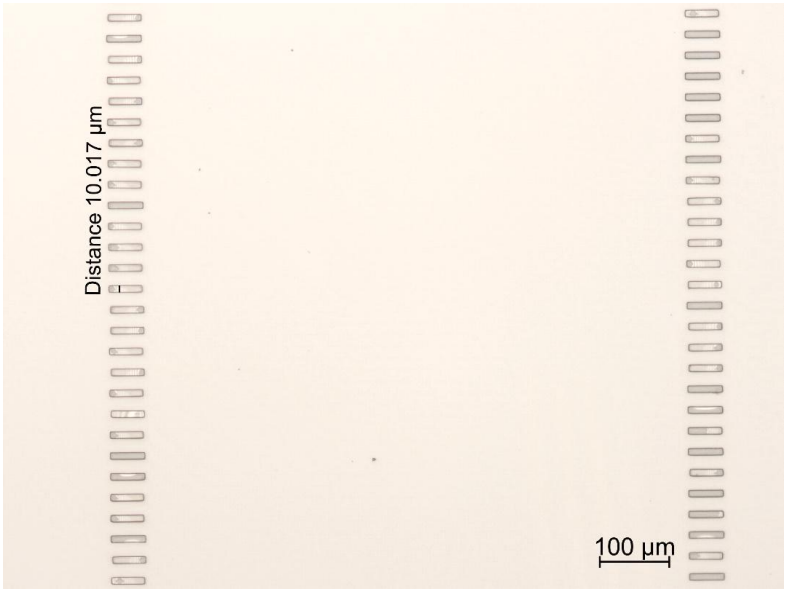

Source: Author.

In the first design proposed, the distance between the main channel and the perfusion microchannels was established as 30 µm. As the microchannel height was 240 µm, shown in Figure 19 (a, b), the aspect ratio of this opening resulted in difficulty in developing the SU-8, causing it not to be performed entirely, not exposing the microchannels, as shown in Figure 19 (c). With this problem, this mold cannot be used as it would allow cells to migrate to other microchannels. The result of the first version of the mold is shown in Figure 20.

Figure 19 - Thickness measurement in profilometer, (a) isometric view and (b) top view, and (c) optical microscopy of the microchannels at 5× magnification.

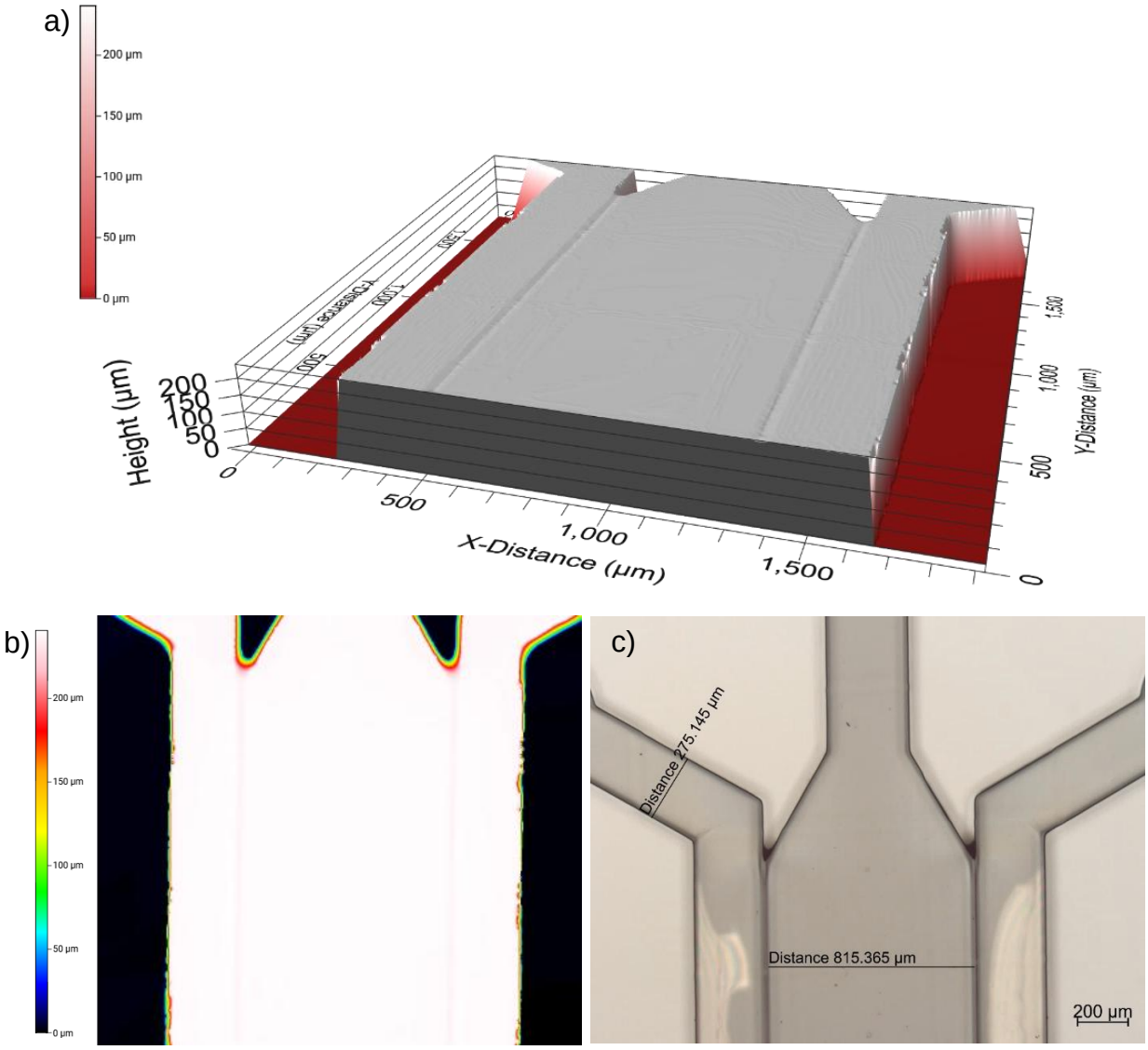

Source: Author.

Figure 20 - Mold Version 1 fabricated on wafer substrate.

Source: Author.

4.3.2.2 Mold Version 2

In version 2, the design was changed to prevent the difficulty of developing the microchannels and avoid exposing the capillaries. The gap between the microchannels was altered to 120 µm and the height to 150 µm. The design of the capillaries was changed according to the increase in the gap between the microchannels, shown in Figure 21.

Figure 21 - Capillaries photolithography.

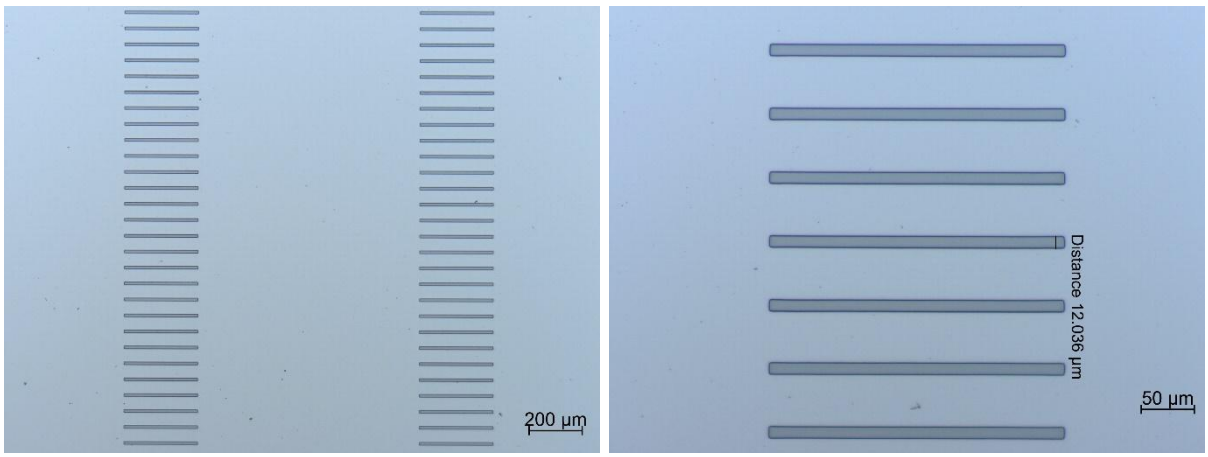

Source: Author.

The spin of the microchannels needed to be changed to achieve the pre-established height, but the difference in this measurement does not impact the device's use. After the capillary photolithography, the microchannels were fabricated. The changes in the process resulted in a complete opening of the gap, as shown in Figure 22, allowing communication without cell migration.

Figure 22 - (a) Profilometry of mold version 2. Microchannels photolithography at (a) 5× magnification and (b) 10× magnification.

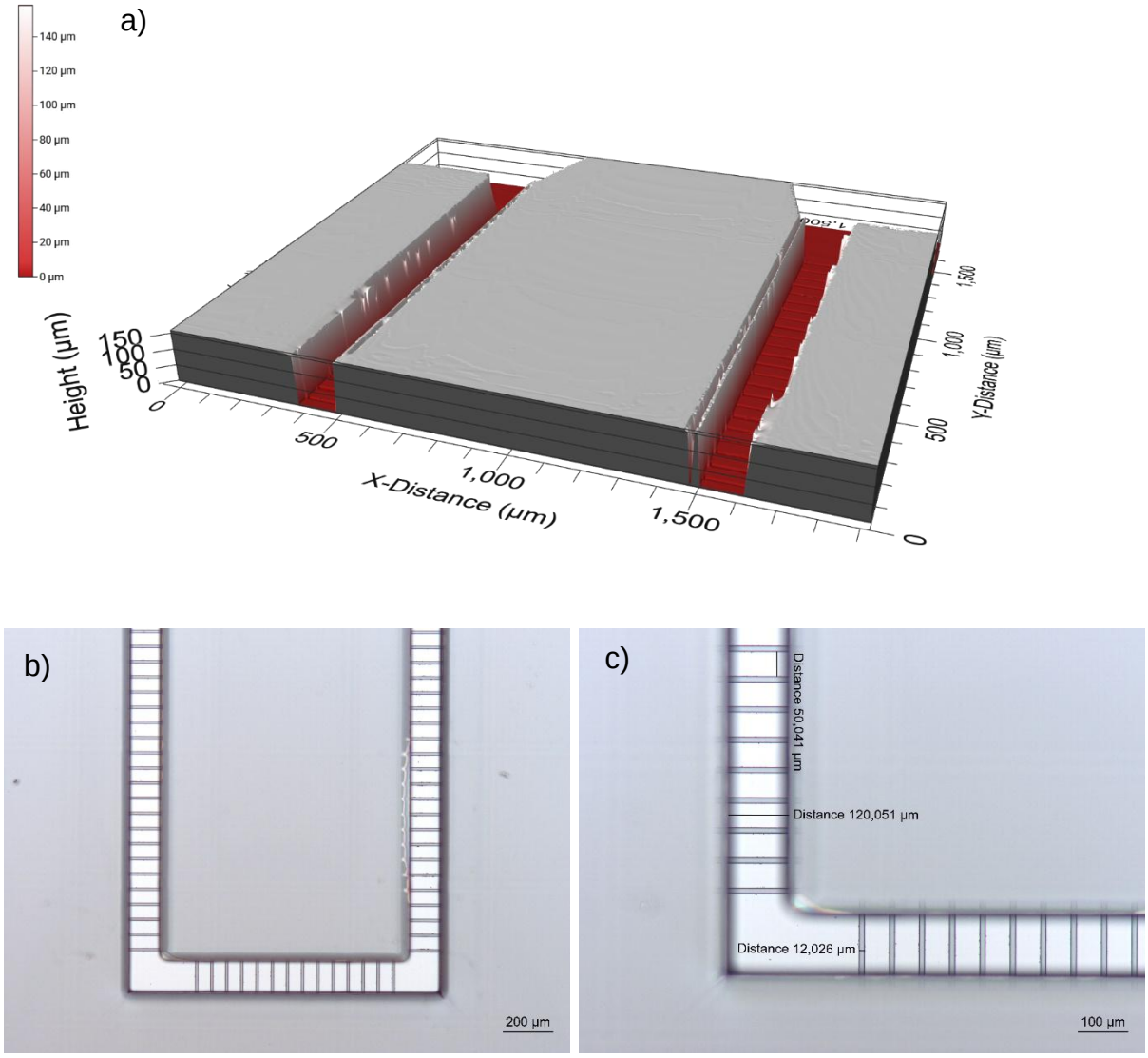

Source: Author.

Figure 23 shows the result of the mold fabrication following the implementation of the necessary adjustments.

Figure 23 - Mold Version 2 fabricated.

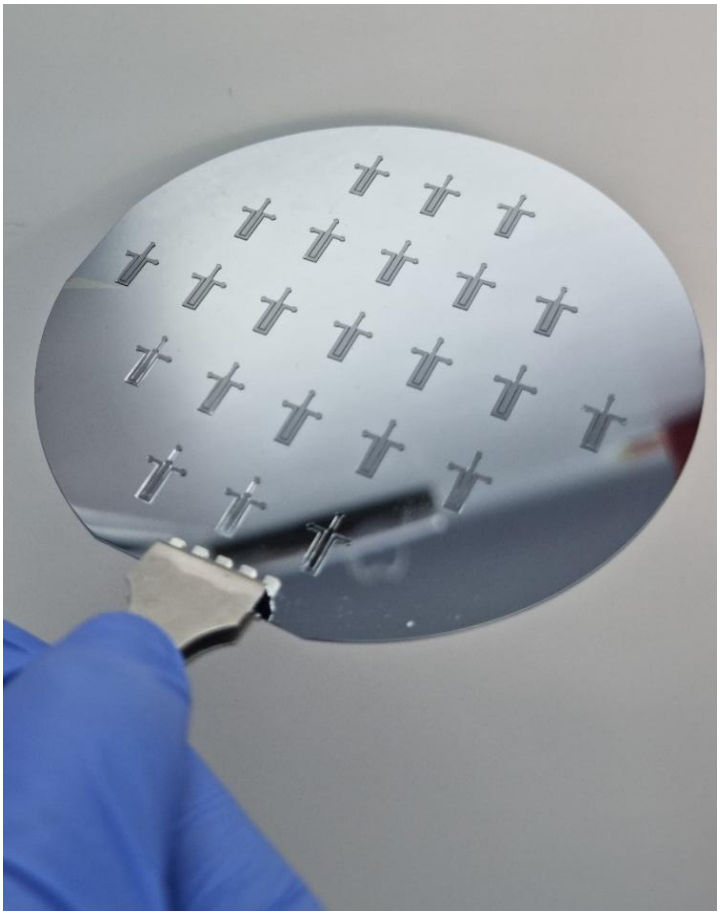

Source: Author.

4.3.3 Microchannel Fabrication and Assembly

After the mold is fabricated, the PDMS microchannels are performed. Following the proposed methodology, the PDMS is mixed with the curing agent and deposited on the mold. Afterward, the bubbles are removed with a vacuum, and the PDMS is cured. This method successfully fabricated the microchannels of the liver-on-a-chip, meeting the requirements shown in Figure 24.

Figure 24 - Microchannels fabrication with mold version 2.

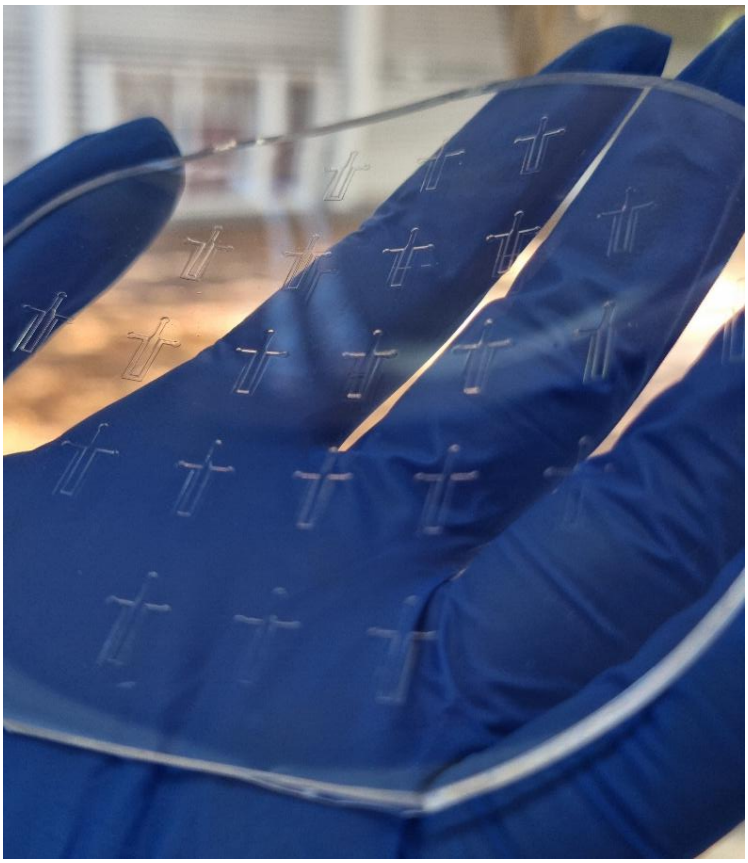

Source: Author.

For the assembly, the microchannels underwent a cleaning process in acetone and were rinsed with ultrapure water. Subsequently, they were immersed in isopropyl alcohol, rinsed once more, and dried using nitrogen. The PDMS microchannels and electrodes were subjected to O_2 plasma and attached with manual pressure using a stereo microscope for alignment. The outcome of the liver-on-a-chip assembly was successful, as shown in Figure 25.

Figure 25 - (a) and (b) Liver-on-a-chip after transfer.

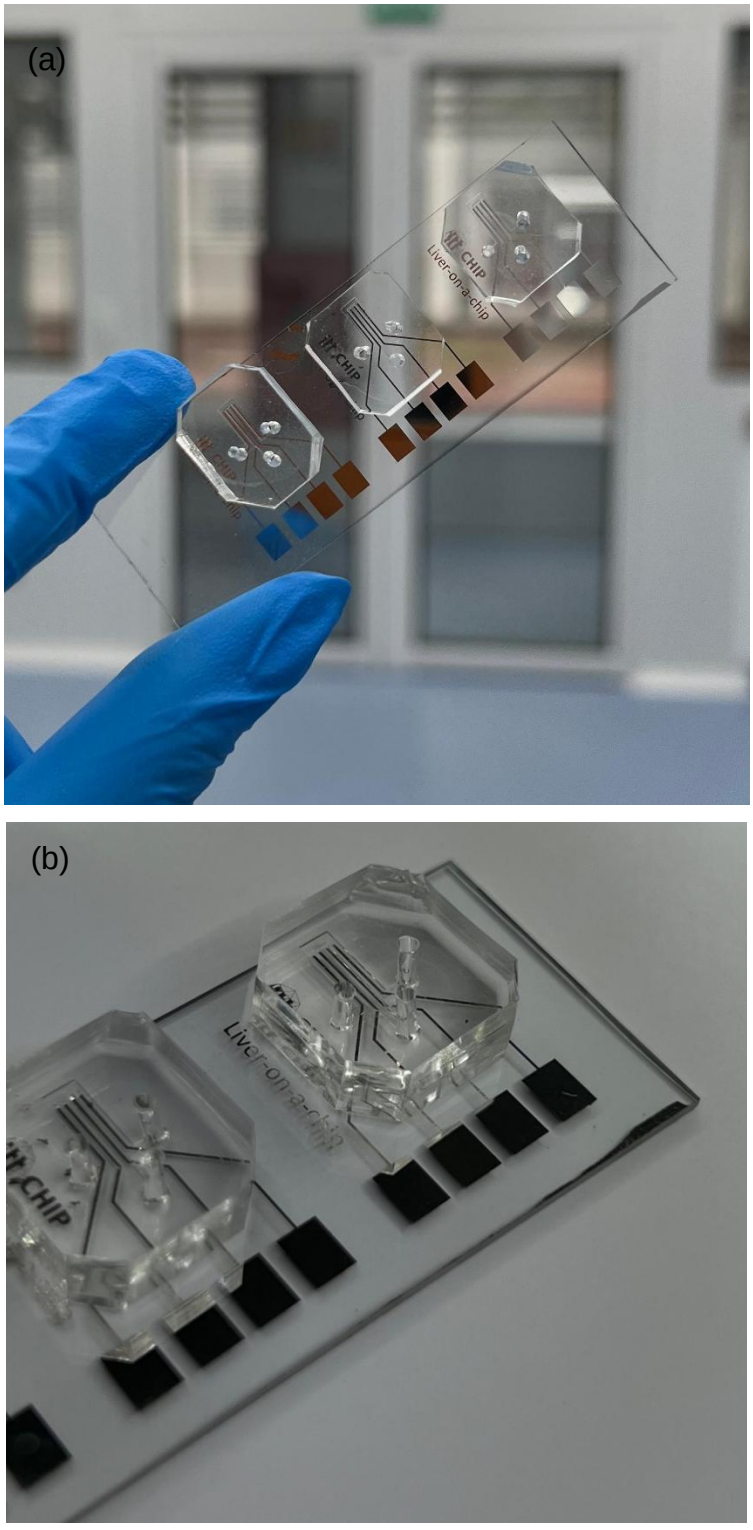

Source: Author.

4.3.4 Cell Culture

HepG2 cells cultured within the microfluidic device demonstrated progressive adhesion, proliferation, and distribution over time under dynamic perfusion conditions. On Day 1, cells appeared evenly distributed but showed minimal adhesion to the chip surface, Figure 26. By Day 3, a noticeable increase in cell density and attachment was observed, with cells beginning to cluster along the microchannel walls. On Day 6, the cells continued to proliferate, forming a confluent monolayer along the endothelial-like microchannels. By Day 9, the cell layer appeared stable and dense, indicating successful long-term culture under perfusion. The results suggest that the microfluidic platform effectively supported HepG2 cell viability and proliferation throughout the experiment, simulating the in vivo hepatic environment.

Figure 26 - Liver-on-a-chip cell culture.

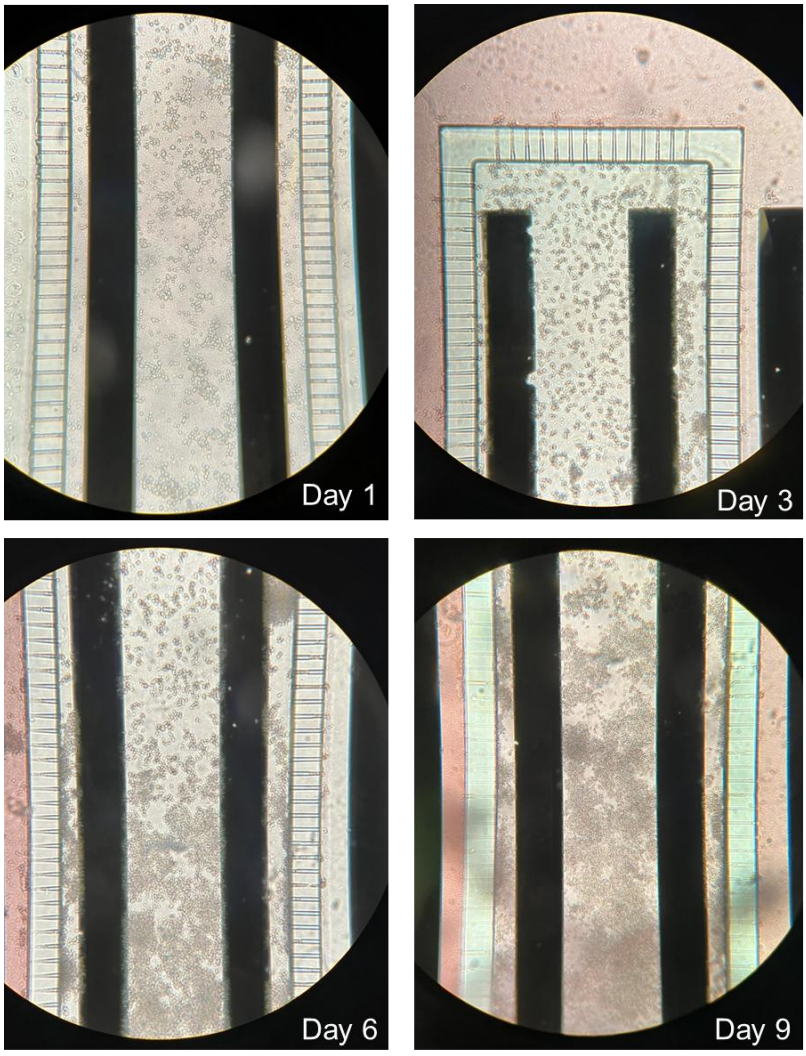

Source: Author.

4.3.5 Electrochemical Impedance Spectroscopy

Figure 27 shows the electrode characterization in PBS solution analyzed using Nyquist and Bode plots. The results provide insight into the electrodes' baseline electrochemical behavior before cell seeding.

Figure 27 - Electrode characterization of the electrodes with PBS: (a) Nyquist plot and (b) Bode plot.

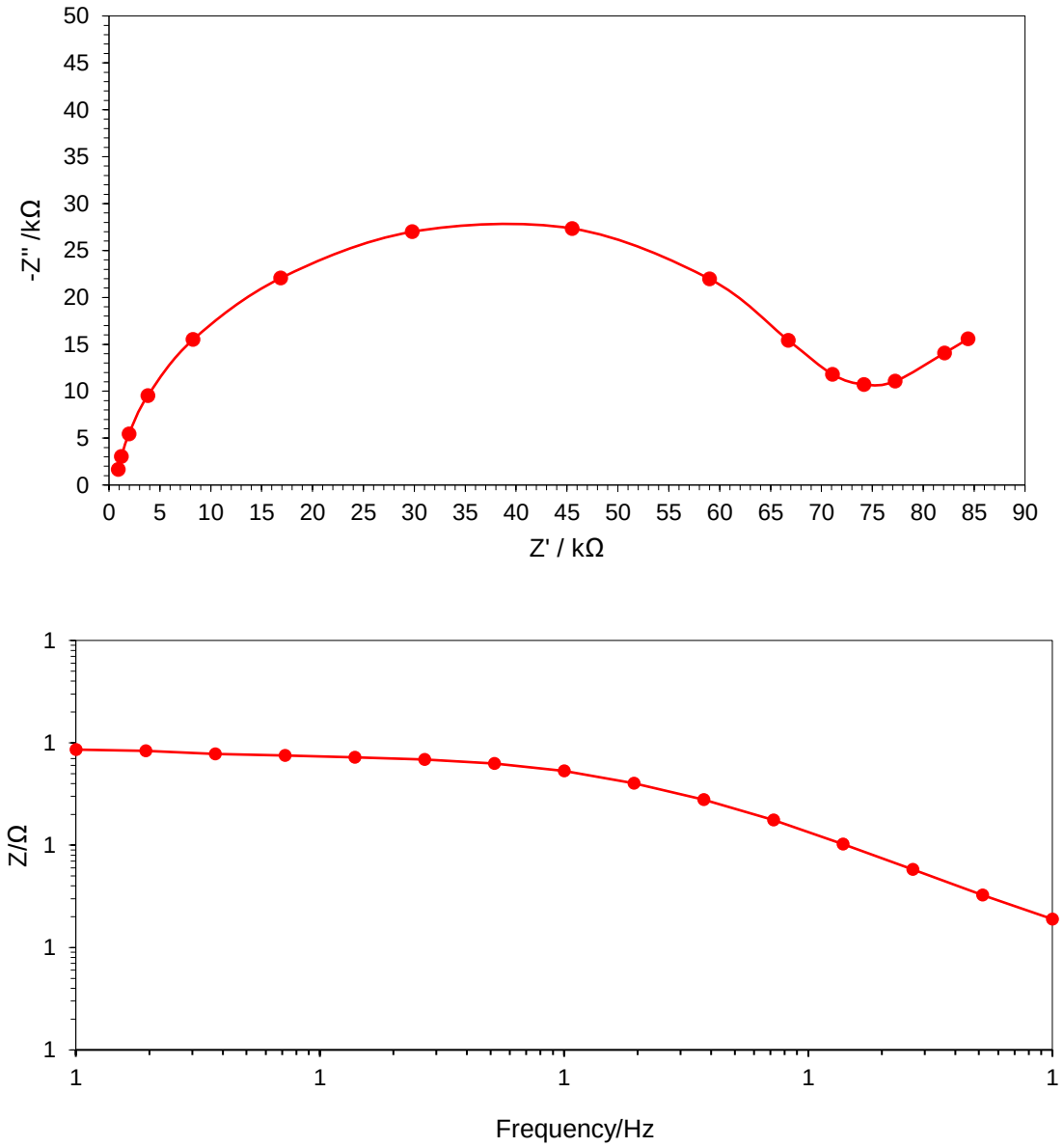

Source: Author.

The Nyquist plot shows a semicircular profile, which is characteristic of an electrochemical system with both resistive and capacitive components. The semicircle observed in the plot indicates the presence of charge transfer resistance (Rct) and a

double-layer capacitance (Cdl) at the electrode-electrolyte interface. The peak of the semicircle is around 60 kΩ, suggesting moderate charge transfer resistance when in contact with PBS. The slight increase at the end of the plot suggests some diffusion-limited processes occurring at lower frequencies, but the profile is predominantly capacitive, confirming the stability of the electrodes in PBS (MAGAR, HASSAN; MULCHANDANI, 2021; ORAZEM; TRIBOLLET, 2011).

The Bode plot presents the impedance magnitude (Z/Ω) as a function of frequency. The plot shows that the impedance remains stable at around 10^5 Ω across a wide frequency range (from 0.1 Hz to 1 kHz), which indicates a low-resistance interface with PBS. This stable behavior confirms that the electrodes are suitable for cell culture impedance measurements, providing reliable baseline readings.

The Nyquist plots in Figure 28 depict the electrical impedance characteristics of a liver-on-a-chip system over several days. The real (Z') and imaginary (-Z'') components of impedance were measured at multiple time points, providing insights into the condition and viability of the liver cell culture throughout the experiment. Each curve represents the system’s response under specific conditions: different culture days, phosphate-buffered saline (PBS) as a control, and post-trypsinization. Monitoring impedance over time enables the verification of cell adhesion, proliferation, and viability, with the PBS and post-trypsinization curves serving as baseline references to separate cellular effects from background signals. This approach validates the dynamic cell culture environment and supports the ongoing assessment of culture stability and health (GUO; ZHU, 2016; OPITZ et al., 2019; WU et al., [s.d.]; YANG et al., 2021).

The data suggests that the liver cells undergo significant changes in electrical properties as the culture matures. On Day 1, the impedance curve (shown in magenta) reaches its highest value, suggesting the presence of a strong electrical barrier formed by intact cell membranes and tight junctions between liver cells. As the culture progresses, the impedance gradually decreases, as seen in the curves for Days 2, 3, 6, 9, and 14. This reduction in impedance may result from factors such as cell death, extracellular matrix degradation, or weakening of cell junctions. These changes reflect the natural aging process and a possible decline in the functionality of the liver cells within the chip, providing valuable insights into the health and viability of the culture over time (JIANG et al., 2024; LAUFER et al., 2010; WANG et al., 2024).

Figure 28 - Nyquist plots with the impedance response of the liver-on-a-chip system under various conditions.

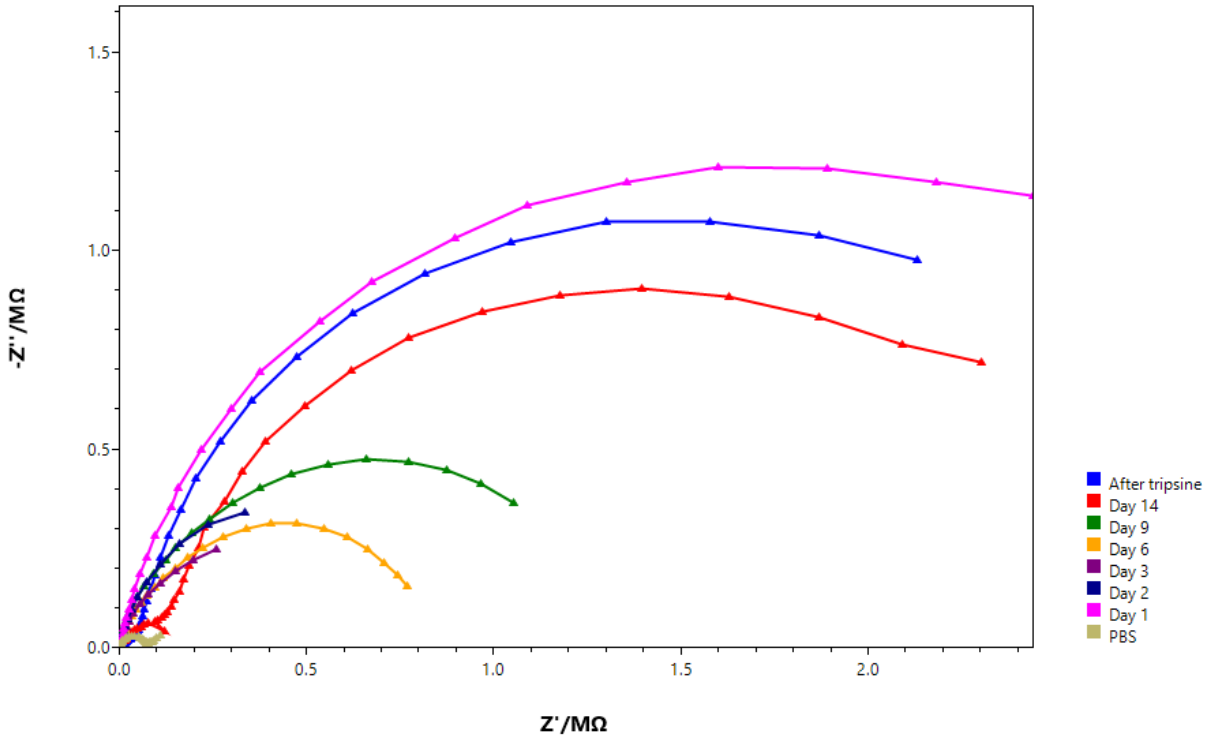

Source: Author.

The PBS curve, representing the control condition without liver cells, shows the lowest impedance values across the entire frequency spectrum. Since the PBS impedance reflects only the electrical properties of the medium without any cellular contribution, it highlights the effect of the cellular layer in the other samples. The higher impedance observed in the cell-containing samples confirms the role of the cellular layer in impeding electrical current, a characteristic associated with viable and healthy cells. This comparison underscores the influence of live cells on the overall impedance, validating the system's ability to monitor cell culture integrity and health.

An important feature in this analysis is the curve labeled "After trypsin," representing the system’s response following the application of trypsin. Trypsin, an enzyme used to detach cells from surfaces by breaking down cell adhesion molecules, is highly relevant in this experiment as it disrupts the cell layer, allowing for a direct assessment of the cellular contribution to the impedance response. The resulting decrease in impedance suggests that the liver cell layer was significantly disrupted post-trypsinization, reducing the impedance barrier formed by the intact cell

membranes. This observation supports the hypothesis that the integrity of the cell layer is crucial to the impedance characteristics of the system, highlighting impedance as an effective indicator of cell layer cohesion and stability. Trypsinization thus serves as a validation step, confirming that changes in impedance over time reflect biological processes such as cell adhesion, growth, and disruption rather than just alterations in the medium or device.

4.3.6 Frequency-Dependent Behavior of the Liver Cell Culture

The Bode plots shown in Figure 29 provide an additional perspective on the evolution of the liver-on-a-chip system by illustrating the magnitude of impedance across a range of frequencies. This plot complements the Nyquist plot by offering a clearer understanding of how impedance varies with frequency, revealing more detailed information about the system's electrical properties. The Bode plot is particularly relevant because it allows for the assessment of both the magnitude and phase of the impedance response, which are influenced by different aspects of the cell culture, such as cell adhesion, proliferation, and the integrity of the cell layer. By comparing the Bode plots for different experimental conditions, including various days of cell culture, PBS as a control, and post-trypsinization, we gain deeper insights into how the liver cell layer evolves and how it contributes to the overall impedance response. This frequency-dependent analysis enhances our understanding of the dynamic behavior of the liver-on-a-chip system, making it a valuable tool for monitoring cell health and culture stability.

In the low-frequency range (below 1 Hz), the impedance values for all conditions remain relatively high, especially for the early time points (e.g., Day 1 and Day 2). This high impedance indicates that the liver cells are presenting a significant barrier to the flow of electric current, which is characteristic of healthy, intact cell membranes that behave like capacitors due to their bilayer structure. The elevated impedance at low frequencies reflects the polarization effects of the cell membranes and the relatively large capacitance they contribute.

Figure 29 - Bode plots with the frequency-dependent impedance characteristics of the liver-on-a-chip system over several days of culture.

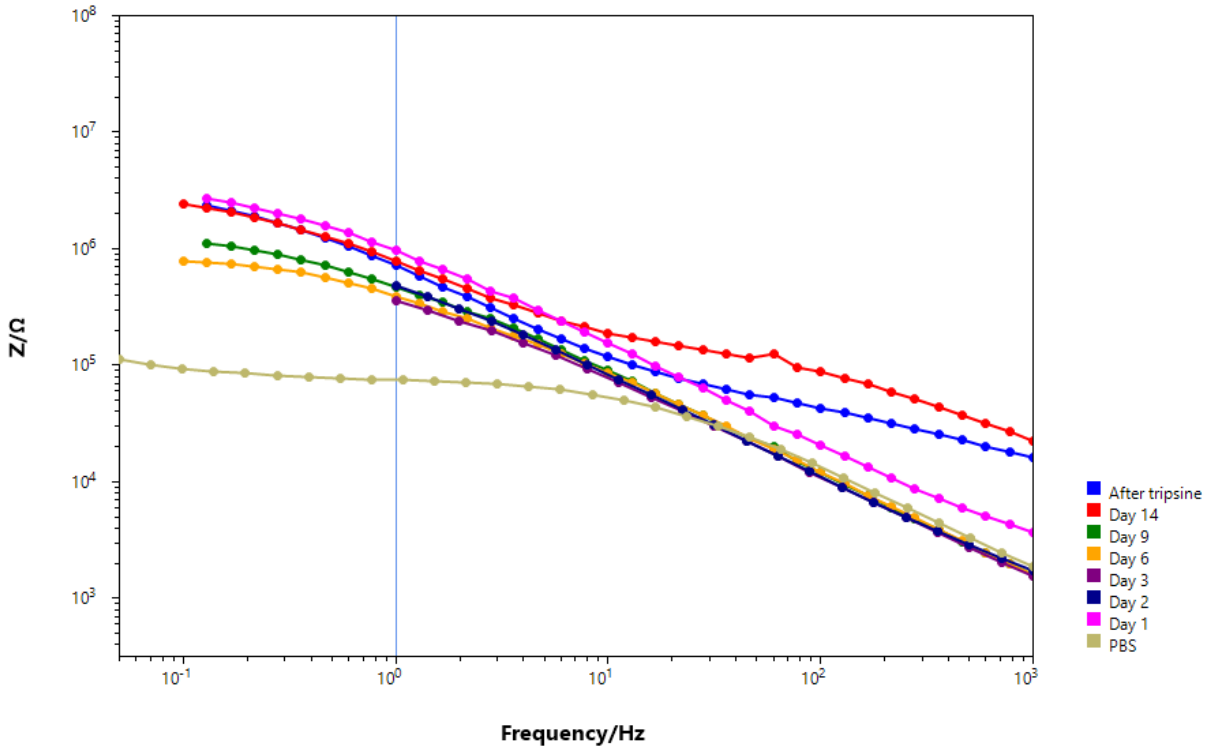

Source: Author.

As the frequency increases, the impedance decreases steadily across all experimental conditions, which is typical of capacitive behavior. In biological systems, impedance generally drops as the applied frequency rises because the cell membranes' ability to impede current diminishes as their capacitive reactance decreases. This frequency dependence is consistent across all days of the experiment, although it becomes less pronounced at later stages (e.g., Day 9 and Day 14), where the overall impedance is lower compared to earlier time points. These changes suggest that, as the culture matures, the cell layer may undergo alterations in membrane integrity or cellular interactions, reducing the ability to impede electrical current at low and high frequencies. (STUPIN et al., 2020).

4.3.7 Changes in Impedance Over Time

The distinct curves for different days of culture in Figure 29 illustrate a progressive decrease in impedance as the culture matures. Day 1 (magenta) and Day

2 (purple) curves exhibit the highest impedance at low frequencies, indicating that the liver cells are in a healthy, functional state, with intact cell membranes and strong tight junctions. However, between Day 1 and Day 2, there was a sharp drop in impedance (~49% at 100 Hz and ~85% at 1 kHz), suggesting an initial adaptation phase, where cells were adhering to the surface and adjusting to the microfluidic environment. This observation is supported by the microscopic image of day 1 in Figure 26, where cells appear dispersed, indicating that adhesion is still in progress.

Between Day 2 and Day 3, impedance at 100 Hz continued to decrease (~85%). Still, at 1 kHz, it increased by approximately 165%, which may indicate changes in cell morphology, improved adhesion, or the formation of stronger cell-cell junctions. This can be seen in Figure 26, day 3, where a noticeable increase in cell density is observed, suggesting enhanced adhesion and early proliferation along the microchannel walls.

From Day 3 to Day 9, the impedance values remained relatively stable, with only minor fluctuations (~2.6% at Day 6 and ~0.06% at Day 9), suggesting that the culture had reached a steady-state phase, where cells maintained a consistent level of adhesion and proliferation. The microscopic images of Day 6 and Day 9 confirm this trend, showing an increasingly confluent monolayer of cells. The impedance stability during this period suggests that cells were well-established in the microenvironment, forming an effective biological barrier within the chip.

A significant shift occurred on Day 14, where impedance increased by 1321% compared to Day 9. This dramatic increase may be associated with cell overgrowth, the formation of a dense monolayer, or modifications in the extracellular matrix, which altered the electrical properties of the system. Despite this increase, the overall impedance trend at low frequencies suggests a gradual degradation of membrane integrity and the loss of tight junctions between cells. The lower impedance at these later time points likely corresponds to increased permeability, cell death, or disruption of cellular interactions, leading to a reduced overall electrical barrier and signaling a decline in the health and functionality of the cell layer.

Finally, the impedance dropped by approximately 28.7% after trypsinization, confirming that the enzymatic treatment effectively detached the cells from the surface. This result validates impedance-based monitoring as a reliable technique for tracking cell adhesion, proliferation, and culture stability over time. The impedance variations observed across different time points align with expected biological behaviors,

reinforcing the potential of this liver-on-a-chip platform for real-time, non-invasive monitoring of hepatic cells.

4.3.8 Control and Post-Trypsinization Effects

The PBS control (brown) consistently exhibits the lowest impedance values across the frequency spectrum, as expected, since PBS lacks the cellular components that contribute to the impedance barrier. It serves as a baseline for understanding the liver-on-a-chip system's behavior in the absence of cells.

The post-trypsinization curve (blue) shows a significant decrease in impedance compared to all other conditions, particularly at low frequencies. This result aligns with the expected effect of trypsin, which enzymatically digests proteins responsible for cell adhesion, leading to cell detachment and disruption of the cellular barrier. The sharp decrease in impedance post-trypsinization confirms the substantial disruption of the cell layer, reducing its contribution to the overall impedance of the system.

The Bode plot further supports the findings from the Nyquist plot, showing an apparent decline in impedance as the liver cell culture ages. The high initial impedance on Days 1 and 2 indicates a well-formed, functional cell layer, while the lower impedance observed on later days reflects the degradation of cell membrane integrity. The PBS control provides a baseline for comparison, and the post-trypsinization data highlights the impact of enzymatic treatment on the cell layer’s disruption. This analysis offers valuable insights into the frequency-dependent electrical behavior of liver cells in a liver-on-a-chip system, revealing their gradual decline over time.

5 CONCLUSION

Developing microfabrication techniques for creating a liver-on-a-chip device significantly advances biomedical engineering and drug testing. This study successfully developed and characterized a liver-on-a-chip device integrating microfabricated electrodes for real-time, label-free monitoring of hepatic cell culture behavior. Firstly, the device was modeled, considering both geometric and usability aspects, ensuring that the microfluidic architecture supported proper perfusion, cell adhesion, and real-time monitoring capabilities. Fluidic and electrical simulations were conducted to assess the system's performance, optimizing the microchannel design for uniform flow distribution and ensuring the electrodes could effectively detect cellular activity. By integrating microfluidic channels with embedded electrodes, this work establishes a robust platform for in-depth exploration of liver cell behavior within a microenvironment that closely mimics physiological conditions. This thesis demonstrates the effective use of microfabrication methods—such as photolithography, soft lithography, and sputtering—to build an advanced microenvironment that addresses key limitations in current preclinical testing, particularly those reliant on static 2D cell cultures and animal models.

The manufacturing process was developed to fabricate both microchannels and electrodes, addressing the challenges of capillary deformation, adhesion, and reproducibility. The refined fabrication protocol led to a functional prototype that met the established design criteria, demonstrating biocompatibility and effective integration of microfluidics and electronics. Cell culture experiments validated the system’s ability to support HepG2 cell adhesion, proliferation, and viability under controlled perfusion conditions. Applying electrical stimuli allowed for assessing its effects on cell function, with electrochemical impedance spectroscopy (EIS) proving an effective, non-invasive technique for monitoring dynamic cellular changes.

The liver-on-a-chip technology designed in this study offers several advantages over traditional models. By providing a dynamic, controlled environment where cells can experience nutrient flow, waste removal, and electrical stimulus, the device better replicates the natural conditions found in vivo. Preliminary results confirmed that the fabrication successfully created microchannels and electrodes that met the required specifications. The integration of impedance spectroscopy for real-time monitoring of

cell culture processes further enhances the system, providing an effective non-invasive method to evaluate cell behavior and device functionality over time.

While this project provides a solid foundation for liver-on-a-chip devices, future research should aim to optimize the biological performance of the system further. Continued studies are required to refine cell culture conditions, extend the range of tested voltages, and explore the effects of prolonged electrical stimulation on liver cells. Incorporating more complex liver models, such as multi-cellular systems that mimic various liver cell types, could enhance the predictive power of the device for drug metabolism and toxicity studies.

Ultimately, this thesis contributes to the growing field of organ-on-a-chip technologies by introducing an innovative platform for liver research. The findings suggest that liver-on-a-chip devices can potentially replace animal models in specific areas of drug development, thus supporting the 3Rs principle by reducing reliance on animal testing. With further development, this platform holds great promise for enhancing drug testing accuracy, lowering costs, and providing new insights into liver diseases and personalized medicine.

In conclusion, the electrode-integrated liver-on-a-chip designed in this study was a significant step towards developing more reliable, scalable, and physiologically relevant in vitro models. By bridging the gap between engineering and biology, this device paves the way for more sophisticated research in drug development and liver pathology, bringing us closer to personalized and effective medical treatments.

REFERENCES

AC/DC Module User's Guide. . [s.l: s.n.]. Disponível em: <www.comsol.com/blogs>.

BUNSHAH, R. F.; DESHPANDEY, ; ; C V; DESHPANDEY, C. V. Plasma assisted physical vapor deposition processes: A review. **Journal of Vacuum Science & Technology A**, v. 3, n. 3, p. 553–560, 1 maio 1985.

CHAN, C. Y. et al. A polystyrene-based microfluidic device with threedimensional interconnected microporous walls for perfusion cell culture. **Biomicrofluidics**, v. 8, n. 4, 1 jul. 2014.

CHELUVAPPA, R.; SCOWEN, P.; ERI, R. **Ethics of animal research in human disease remediation, its institutional teaching; and alternatives to animal experimentation**. **Pharmacology Research and Perspectives**, 2017.

CONG, Y. et al. Drug Toxicity Evaluation Based on Organ-on-a-chip Technology: A Review. **Micromachines 2020, Vol. 11, Page 381**, v. 11, n. 4, p. 381, 3 abr. 2020.

DE LEÓN, S. E.; PUPOVAC, A.; MCARTHUR, S. L. Three-Dimensional (3D) cell culture monitoring: Opportunities and challenges for impedance spectroscopy. **Biotechnology and Bioengineering**, v. 117, n. 4, p. 1230–1240, 1 abr. 2020.

DENG, J. et al. Engineered Liver-on-a-Chip Platform to Mimic Liver Functions and Its Biomedical Applications: A Review. **Micromachines**, v. 10, n. 10, 1 out. 2019.

DENG, T. et al. Prototyping of masks, masters, and stamps/molds for soft lithography using an office printer and photographic reduction. **ACS Publications**, v. 72, n. 14, p. 3176–3180, 15 jul. 2000.

DESPA, M. S.; KELLY, K. W.; COLLIER, J. R. **Injection molding of polymeric LIGA HARMs**. [s.l: s.n.].

DUFFY, D. C. et al. Rapid prototyping of microfluidic systems in poly(dimethylsiloxane). **Analytical Chemistry**, v. 70, n. 23, p. 4974–4984, 1 dez. 1998.

EHRLICH, A. et al. **Challenges and Opportunities in the Design of Liver-on-Chip Microdevices**. **Annual Review of Biomedical Engineering**Annual Reviews Inc., , 2019.

EVERITT, J. I. The Future of Preclinical Animal Models in Pharmaceutical Discovery and Development. **Toxicologic Pathology**, 2015.

FONSECA, M. A. M. et al. Bioética na Pesquisa Engenharia Biomédica: diminuição do uso de animais em experimentos científicos. **Revista Interdisciplinar de Pesquisa em Engenharia**, 2018.

FONTANA, F. et al. Requirements for Animal Experiments: Problems and Challenges. **Small**, v. 17, n. 15, p. 2004182, 1 abr. 2021.

Fundamentals and Applications of Microfluidics, Third Edition | Artech books | IEEE Xplore. Disponível em: <https://ieeexplore.ieee.org/document/9098772>. Acesso em: 5 out. 2022.

GHAEMMAGHAMI, A. M. et al. Biomimetic tissues on a chip for drug discovery. **Drug Discovery Today**, v. 17, n. 3–4, p. 173–181, fev. 2012.

GORI, M. et al. Investigating nonalcoholic fatty liver disease in a liver-on-a-chip microfluidic device. **PLoS ONE**, v. 11, n. 7, 1 jul. 2016.

GUO, X.; ZHU, R. Controllable in-situ cell electroporation with cell positioning and impedance monitoring using micro electrode array. **Scientific Reports**, v. 6, n. 1, 10 ago. 2016.

Guyton and Hall Textbook of Medical Physiology. . [s.l: s.n.]. Disponível em: <http://avaxho.me/blogs/ChrisRedfield>.

HILDEBRANDT, C. et al. Detection of the osteogenic differentiation of mesenchymal stem cells in 2D and 3D cultures by electrochemical impedance spectroscopy. **Journal of Biotechnology**, v. 148, n. 1, p. 83–90, jul. 2010.

ISHIDA, S. **Organs-on-a-chip: Current applications and consideration points for in vitro ADME-Tox studies**. **Drug Metabolism and Pharmacokinetics**, 2018.

JIANG, H. et al. NAFLD's Predisposion: insight from phenome-wide association and Mendelian Randomization. 6 ago. 2024.

JO, B. H. et al. Three-dimensional micro-channel fabrication in polydimethylsiloxane (PDMS) elastomer. **Journal of Microelectromechanical Systems**, v. 9, n. 1, p. 76–81, mar. 2000.

KAVAND, H. et al. Advanced Materials and Sensors for Microphysiological Systems: Focus on Electronic and Electrooptical Interfaces. **Advanced Materials**, v. 34, n. 17, p. 2107876, 1 abr. 2022.

KHAZALI, A. S.; CLARK, A. M.; WELLS, A. A Pathway to Personalizing Therapy for Metastases Using Liver-on-a-Chip Platforms. **Stem Cell Reviews and Reports 2017 13:3**, v. 13, n. 3, p. 364–380, 19 abr. 2017.

KHETANI, S. R. et al. Microengineered Liver Tissues for Drug Testing. **SLAS Technology**, v. 20, n. 3, p. 216–250, 3 jun. 2015.

KIM, H. J. et al. Contributions of microbiome and mechanical deformation to intestinal bacterial overgrowth and inflammation in a human gut-on-a-chip. **Proceedings of the National Academy of Sciences of the United States of America**, 2016.

KIM, S. et al. Engineering of functional, perfusable 3D microvascular networks on a chip. **Lab on a Chip**, v. 13, n. 8, p. 1489–1500, 2013.

KIMURA, H.; SAKAI, Y.; FUJII, T. **Organ/body-on-a-chip based on microfluidic technology for drug discovery**. **Drug Metabolism and Pharmacokinetics**, 2018.

LANDI, M. S.; SHRIVER, A. J.; MUELLER, A. **Consideration and checkboxes: Incorporating ethics and science into the 3Rs**. **Journal of the American Association for Laboratory Animal Science**, 2015.

LAUFER, S. et al. Electrical impedance characterization of normal and cancerous human hepatic tissue. **Physiological Measurement**, v. 31, n. 7, p. 995–1009, 2010.

LEE, B. K. et al. Electrical characterization of the platinum/YSZ interfaces in SOFCs via micro-contact impedance spectroscopy. **Journal of Electroceramics**, v. 17, n. 2–4, p. 735–739, dez. 2006.

LEE, H.; CHO, D. W. One-step fabrication of an organ-on-a-chip with spatial heterogeneity using a 3D bioprinting technology. **Lab on a Chip**, v. 16, n. 14, p. 2618–2625, 5 jul. 2016.

LEE, J. et al. Design and fabrication of CD-like microfluidic platforms for diagnostics: Polymer-based microfabrication. **Biomedical Microdevices**, v. 3, n. 4, p. 339–351, 2001.

LEE, S. H.; JUN, B. H. **Advances in dynamic microphysiological organ-on-a-chip: Design principle and its biomedical application**. **Journal of Industrial and Engineering Chemistry**Korean Society of Industrial Engineering Chemistry, , 25 mar. 2019.

LEE, S.-J. JOHN.; SUNDARARAJAN, NARAYANAN. Microfabrication for microfluidics. p. 262, [s.d.].

LI, Y. et al. **New developments of ti-based alloys for biomedical applications**. **Materials**MDPI AG, , 2014.

MADOU, M. J. Fundamentals of microfabrication and nanotechnology. 2012.

MAGAR, H. S.; HASSAN, R. Y. A.; MULCHANDANI, A. Electrochemical Impedance Spectroscopy (EIS): Principles, Construction, and Biosensing Applications. **Sensors (Basel, Switzerland)**, v. 21, n. 19, p. 6578, 1 out. 2021.

MANZ, A. et al. Planar chips technology for miniaturization and integration of separation techniques into monitoring systems: Capillary electrophoresis on a chip. **Journal of Chromatography A**, v. 593, n. 1–2, p. 253–258, 28 fev. 1992.

MAO, M. et al. The Emerging Frontiers and Applications of High-Resolution 3D Printing. **Micromachines 2017, Vol. 8, Page 113**, v. 8, n. 4, p. 113, 1 abr. 2017.

MATA, A.; FLEISCHMAN, A. J.; ROY, S. Characterization of Polydimethylsiloxane (PDMS) Properties for Biomedical Micro/Nanosystems. **Biomedical Microdevices**, v. 7, n. 4, p. 281–293, 2005a.

MATA, A.; FLEISCHMAN, A. J.; ROY, S. Characterization of polydimethylsiloxane (PDMS) properties for biomedical micro/nanosystems. **Biomedical microdevices**, v. 7, n. 4, p. 281–293, 1 dez. 2005b.

MATTOX, D. M. Physical vapor deposition (PVD) processes. **Metal Finishing**, v. 100, n. 1 SUPPL., p. 394–408, 1 jan. 2002.

MCDONALD, J. C.; WHITESIDES, G. M. Poly(dimethylsiloxane) as a material for fabricating microfluidic devices. **Accounts of chemical research**, v. 35, n. 7, p. 491–499, 2002.

M.M.ABDELRAHMAN. Study of Plasma and Ion Beam Sputtering Processes. **Journal of Physical Science and Application**, v. 5, n. 2, 28 fev. 2015.

MOREIRA, A. et al. Advanced In Vitro Lung Models for Drug and Toxicity Screening: The Promising Role of Induced Pluripotent Stem Cells. **Advanced Biology**, p. 2101139, 27 dez. 2021.

NGUYEN, H.; HOANG, T. Numerical Simulation of Laminar Flow Through a Pipe using COMSOL Multiphysics. **International Journal of Scientific & Engineering Research**, v. 8, n. 6, 2017.

O'NEILL, R. D. et al. **Comparisons of platinum, gold, palladium and glassy carbon as electrode materials in the design of biosensors for glutamate**. Biosensors and Bioelectronics. **Anais**...15 jun. 2004.

OPITZ, C. et al. Rapid determination of general cell status, cell viability, and optimal harvest time in eukaryotic cell cultures by impedance flow cytometry. **Applied Microbiology and Biotechnology**, v. 103, n. 20, p. 8619–8629, 1 out. 2019.

ORAZEM, M. E. .; TRIBOLLET, BERNARD. Electrochemical Impedance Spectroscopy. p. 498, 2011.

QIU, L. et al. Recent advances in liver-on-chips: Design, fabrication, and applications. **Smart Medicine**, v. 2, n. 1, p. e20220010, 1 fev. 2023.

QUERO, J. M.; PERDIGONES, F.; ARACIL, C. Microfabrication technologies used for creating smart devices for industrial applications. **Smart Sensors and MEMS: Intelligent Sensing Devices and Microsystems for Industrial Applications: Second Edition**, p. 291–311, 1 jan. 2018.

RAMADAN, Q.; ZOUROB, M. **Organ-on-a-chip engineering: Toward bridging the gap between lab and industry**. **Biomicrofluidics**American Institute of Physics Inc., , 1 jul. 2020.

RENATA, N.; MOREIRA, P. Estudo de várias propriedades mecânicas do polidimetilsiloxano (PDMS) usado em dispositivos biomédicos. 2013.

RUSSELL, W. M. S.; BURCH, R. L. **The principles of humane experimental technique**. [s.l.] Methuen, 1959.

SCHNEIDER, F. et al. **Mechanical properties of silicones for MEMS**. Journal of Micromechanics and Microengineering. **Anais**...1 jun. 2008.

SOSA-HERNÁNDEZ, J. E. et al. Organs-on-a-Chip Module: A Review from the Development and Applications Perspective. **Micromachines**, v. 9, n. 10, 22 out. 2018.

SRINIVASAN, B. et al. TEER Measurement Techniques for In Vitro Barrier Model Systems. **SLAS Technology**, v. 20, n. 2, p. 107–126, 1 abr. 2015.

STUPIN, D. D. et al. Bio-Impedance Spectroscopy: Basics and Applications. 2020.

THESES, G.; WEERASINGHE, H. C. **Electrical Characterization Of Metal-To-Insulator Transition In Iron Silicide Thin Films On Silicon Substrates**. [s.l: s.n.]. Disponível em: <https://scholarcommons.usf.edu/etd>.

THUY, T. N. T.; TSENG, T. T. C. A micro-platinumwire biosensor for fast and selective detection of alanine aminotransferase. **Sensors (Switzerland)**, v. 16, n. 6, 1 jun. 2016.

TSVIRKUN, D. et al. Microvasculature on a chip: study of the Endothelial Surface Layer and the flow structure of Red Blood Cells. **Scientific Reports**, v. 7, n. 1, 24 mar. 2017.

UNGER, M. A. et al. Monolithic microfabricated valves and pumps by multilayer soft lithography. **Science**, v. 288, n. 5463, p. 113–116, 7 abr. 2000.

VACCARI, N. et al. White light spectroscopy for T-cell culture growth monitoring: towards a real-time and sampling free device for ATMPs production. **Journal of Translational Science**, v. 7, n. 6, 2021.

VAN DER HELM, M. W. et al. Lab on a Chip Non-invasive sensing of transepithelial barrier function and tissue differentiation in organs-on-chips using impedance spectroscopy †. v. 19, p. 452, 2019.

WACOGNE, B. et al. Absorption Spectra Description for T-Cell Concentrations Determination and Simultaneous Measurements of Species during Co-Cultures. **Sensors 2022, Vol. 22, Page 9223**, v. 22, n. 23, p. 9223, 27 nov. 2022.

WANG, K. et al. Non-Invasive Detection of Early-Stage Fatty Liver Disease via an On-Skin Impedance Sensor and Attention-Based Deep Learning. **Advanced Science**, v. 11, n. 31, 21 ago. 2024.

WHITESIDES, G. M. The origins and the future of microfluidics. **Nature 2006 442:7101**, v. 442, n. 7101, p. 368–373, 26 jul. 2006.

WU, Z. et al. Potent-By-Design: Amino Acids Mimicking Porous Nanotherapeutics with Intrinsic Anticancer Targeting Properties. **Small**, v. 16, n. 34, [s.d.].

XIA, Y.; WHITESIDES, G. M. **SOFT LITHOGRAPHYAnnu. Rev. Mater. Sci**. [s.l: s.n.]. Disponível em: <www.annualreviews.org>.

YANG, N. et al. Temperature Tolerance Electric Cell-Substrate Impedance Sensing for Joint Assessment of Cell Viability and Vitality. **ACS Sensors**, v. 6, n. 10, p. 3640–3649, 22 out. 2021.

YESTE, J. et al. A compartmentalized microfluidic chip with crisscross microgrooves and electrophysiological electrodes for modeling the blood-retinal barrier. **Lab on a Chip**, v. 18, n. 1, p. 95–105, 7 jan. 2018.

ZAOUK, R.; PARK, B. Y.; MADOU, M. J. Introduction to microfabrication techniques. **Methods in molecular biology (Clifton, N.J.)**, v. 321, p. 5–15, 2006.

ZHANG, Y. S.; ZHANG, Y.-N.; ZHANG, W. Cancer-on-a-chip systems at the frontier of nanomedicine. [s.d.].

ZHU, Y. et al. Microfluidic immobilized enzyme reactors for continuous biocatalysis. **Reaction Chemistry and Engineering**, v. 5, n. 1, p. 9–32, 1 jan. 2020.

AC/DC Module User's Guide. . [s.l: s.n.]. Disponível em: <www.comsol.com/blogs>.

BUNSHAH, R. F.; DESHPANDEY, ; ; C V; DESHPANDEY, C. V. Plasma assisted physical vapor deposition processes: A review. **Journal of Vacuum Science & Technology A**, v. 3, n. 3, p. 553–560, 1 maio 1985.

CHAN, C. Y. et al. A polystyrene-based microfluidic device with threedimensional interconnected microporous walls for perfusion cell culture. **Biomicrofluidics**, v. 8, n. 4, 1 jul. 2014.

CHELUVAPPA, R.; SCOWEN, P.; ERI, R. **Ethics of animal research in human disease remediation, its institutional teaching; and alternatives to animal experimentation**. **Pharmacology Research and Perspectives**, 2017.

CONG, Y. et al. Drug Toxicity Evaluation Based on Organ-on-a-chip Technology: A Review. **Micromachines 2020, Vol. 11, Page 381**, v. 11, n. 4, p. 381, 3 abr. 2020.

DE LEÓN, S. E.; PUPOVAC, A.; MCARTHUR, S. L. Three-Dimensional (3D) cell culture monitoring: Opportunities and challenges for impedance spectroscopy. **Biotechnology and Bioengineering**, v. 117, n. 4, p. 1230–1240, 1 abr. 2020.

DENG, J. et al. Engineered Liver-on-a-Chip Platform to Mimic Liver Functions and Its Biomedical Applications: A Review. **Micromachines**, v. 10, n. 10, 1 out. 2019.

DENG, T. et al. Prototyping of masks, masters, and stamps/molds for soft lithography using an office printer and photographic reduction. **ACS Publications**, v. 72, n. 14, p. 3176–3180, 15 jul. 2000.

DESPA, M. S.; KELLY, K. W.; COLLIER, J. R. **Injection molding of polymeric LIGA HARMs**. [s.l: s.n.].

DUFFY, D. C. et al. Rapid prototyping of microfluidic systems in poly(dimethylsiloxane). **Analytical Chemistry**, v. 70, n. 23, p. 4974–4984, 1 dez. 1998.

EHRLICH, A. et al. **Challenges and Opportunities in the Design of Liver-on-Chip Microdevices**. **Annual Review of Biomedical Engineering**Annual Reviews Inc., , 2019.

EVERITT, J. I. The Future of Preclinical Animal Models in Pharmaceutical Discovery and Development. **Toxicologic Pathology**, 2015.

FONSECA, M. A. M. et al. Bioética na Pesquisa Engenharia Biomédica: diminuição do uso de animais em experimentos científicos. **Revista Interdisciplinar de Pesquisa em Engenharia**, 2018.

FONTANA, F. et al. Requirements for Animal Experiments: Problems and Challenges. **Small**, v. 17, n. 15, p. 2004182, 1 abr. 2021.

Fundamentals and Applications of Microfluidics, Third Edition | Artech books | IEEE Xplore. Disponível em: <https://ieeexplore.ieee.org/document/9098772>. Acesso em: 5 out. 2022.

GHAEMMAGHAMI, A. M. et al. Biomimetic tissues on a chip for drug discovery. **Drug Discovery Today**, v. 17, n. 3–4, p. 173–181, fev. 2012.

GORI, M. et al. Investigating nonalcoholic fatty liver disease in a liver-on-a-chip microfluidic device. **PLoS ONE**, v. 11, n. 7, 1 jul. 2016.

GUO, X.; ZHU, R. Controllable in-situ cell electroporation with cell positioning and impedance monitoring using micro electrode array. **Scientific Reports**, v. 6, n. 1, 10 ago. 2016.

Guyton and Hall Textbook of Medical Physiology. . [s.l: s.n.]. Disponível em: <http://avaxho.me/blogs/ChrisRedfield>.

HILDEBRANDT, C. et al. Detection of the osteogenic differentiation of mesenchymal stem cells in 2D and 3D cultures by electrochemical impedance spectroscopy. **Journal of Biotechnology**, v. 148, n. 1, p. 83–90, jul. 2010.

ISHIDA, S. **Organs-on-a-chip: Current applications and consideration points for in vitro ADME-Tox studies**. **Drug Metabolism and Pharmacokinetics**, 2018.

JIANG, H. et al. NAFLD's Predisposion: insight from phenome-wide association and Mendelian Randomization. 6 ago. 2024.

JO, B. H. et al. Three-dimensional micro-channel fabrication in polydimethylsiloxane (PDMS) elastomer. **Journal of Microelectromechanical Systems**, v. 9, n. 1, p. 76–81, mar. 2000.

KAVAND, H. et al. Advanced Materials and Sensors for Microphysiological Systems: Focus on Electronic and Electrooptical Interfaces. **Advanced Materials**, v. 34, n. 17, p. 2107876, 1 abr. 2022.

KHAZALI, A. S.; CLARK, A. M.; WELLS, A. A Pathway to Personalizing Therapy for Metastases Using Liver-on-a-Chip Platforms. **Stem Cell Reviews and Reports 2017 13:3**, v. 13, n. 3, p. 364–380, 19 abr. 2017.

KHETANI, S. R. et al. Microengineered Liver Tissues for Drug Testing. **SLAS Technology**, v. 20, n. 3, p. 216–250, 3 jun. 2015.

KIM, H. J. et al. Contributions of microbiome and mechanical deformation to intestinal bacterial overgrowth and inflammation in a human gut-on-a-chip. **Proceedings of the National Academy of Sciences of the United States of America**, 2016.

KIM, S. et al. Engineering of functional, perfusable 3D microvascular networks on a chip. **Lab on a Chip**, v. 13, n. 8, p. 1489–1500, 2013.

KIMURA, H.; SAKAI, Y.; FUJII, T. **Organ/body-on-a-chip based on microfluidic technology for drug discovery**. **Drug Metabolism and Pharmacokinetics**, 2018.

LANDI, M. S.; SHRIVER, A. J.; MUELLER, A. **Consideration and checkboxes: Incorporating ethics and science into the 3Rs**. **Journal of the American Association for Laboratory Animal Science**, 2015.

LAUFER, S. et al. Electrical impedance characterization of normal and cancerous human hepatic tissue. **Physiological Measurement**, v. 31, n. 7, p. 995–1009, 2010.

LEE, B. K. et al. Electrical characterization of the platinum/YSZ interfaces in SOFCs via micro-contact impedance spectroscopy. **Journal of Electroceramics**, v. 17, n. 2–4, p. 735–739, dez. 2006.

LEE, H.; CHO, D. W. One-step fabrication of an organ-on-a-chip with spatial heterogeneity using a 3D bioprinting technology. **Lab on a Chip**, v. 16, n. 14, p. 2618–2625, 5 jul. 2016.

LEE, J. et al. Design and fabrication of CD-like microfluidic platforms for diagnostics: Polymer-based microfabrication. **Biomedical Microdevices**, v. 3, n. 4, p. 339–351, 2001.

LEE, S. H.; JUN, B. H. **Advances in dynamic microphysiological organ-on-a-chip: Design principle and its biomedical application**. **Journal of Industrial and Engineering Chemistry**Korean Society of Industrial Engineering Chemistry, , 25 mar. 2019.

LEE, S.-J. JOHN.; SUNDARARAJAN, NARAYANAN. Microfabrication for microfluidics. p. 262, [s.d.].

LI, Y. et al. **New developments of ti-based alloys for biomedical applications**. **Materials**MDPI AG, , 2014.

MADOU, M. J. Fundamentals of microfabrication and nanotechnology. 2012.

MAGAR, H. S.; HASSAN, R. Y. A.; MULCHANDANI, A. Electrochemical Impedance Spectroscopy (EIS): Principles, Construction, and Biosensing Applications. **Sensors (Basel, Switzerland)**, v. 21, n. 19, p. 6578, 1 out. 2021.

MANZ, A. et al. Planar chips technology for miniaturization and integration of separation techniques into monitoring systems: Capillary electrophoresis on a chip. **Journal of Chromatography A**, v. 593, n. 1–2, p. 253–258, 28 fev. 1992.

MAO, M. et al. The Emerging Frontiers and Applications of High-Resolution 3D Printing. **Micromachines 2017, Vol. 8, Page 113**, v. 8, n. 4, p. 113, 1 abr. 2017.

MATA, A.; FLEISCHMAN, A. J.; ROY, S. Characterization of Polydimethylsiloxane (PDMS) Properties for Biomedical Micro/Nanosystems. **Biomedical Microdevices**, v. 7, n. 4, p. 281–293, 2005a.

MATA, A.; FLEISCHMAN, A. J.; ROY, S. Characterization of polydimethylsiloxane (PDMS) properties for biomedical micro/nanosystems. **Biomedical microdevices**, v. 7, n. 4, p. 281–293, 1 dez. 2005b.

MATTOX, D. M. Physical vapor deposition (PVD) processes. **Metal Finishing**, v. 100, n. 1 SUPPL., p. 394–408, 1 jan. 2002.

MCDONALD, J. C.; WHITESIDES, G. M. Poly(dimethylsiloxane) as a material for fabricating microfluidic devices. **Accounts of chemical research**, v. 35, n. 7, p. 491–499, 2002.

M.M.ABDELRAHMAN. Study of Plasma and Ion Beam Sputtering Processes. **Journal of Physical Science and Application**, v. 5, n. 2, 28 fev. 2015.

MOREIRA, A. et al. Advanced In Vitro Lung Models for Drug and Toxicity Screening: The Promising Role of Induced Pluripotent Stem Cells. **Advanced Biology**, p. 2101139, 27 dez. 2021.

NGUYEN, H.; HOANG, T. Numerical Simulation of Laminar Flow Through a Pipe using COMSOL Multiphysics. **International Journal of Scientific & Engineering Research**, v. 8, n. 6, 2017.

O'NEILL, R. D. et al. **Comparisons of platinum, gold, palladium and glassy carbon as electrode materials in the design of biosensors for glutamate**. Biosensors and Bioelectronics. **Anais**...15 jun. 2004.

OPITZ, C. et al. Rapid determination of general cell status, cell viability, and optimal harvest time in eukaryotic cell cultures by impedance flow cytometry. **Applied Microbiology and Biotechnology**, v. 103, n. 20, p. 8619–8629, 1 out. 2019.

ORAZEM, M. E. .; TRIBOLLET, BERNARD. Electrochemical Impedance Spectroscopy. p. 498, 2011.

QIU, L. et al. Recent advances in liver-on-chips: Design, fabrication, and applications. **Smart Medicine**, v. 2, n. 1, p. e20220010, 1 fev. 2023.

QUERO, J. M.; PERDIGONES, F.; ARACIL, C. Microfabrication technologies used for creating smart devices for industrial applications. **Smart Sensors and MEMS: Intelligent Sensing Devices and Microsystems for Industrial Applications: Second Edition**, p. 291–311, 1 jan. 2018.

RAMADAN, Q.; ZOUROB, M. **Organ-on-a-chip engineering: Toward bridging the gap between lab and industry**. **Biomicrofluidics**American Institute of Physics Inc., , 1 jul. 2020.

RENATA, N.; MOREIRA, P. Estudo de várias propriedades mecânicas do polidimetilsiloxano (PDMS) usado em dispositivos biomédicos. 2013.

RUSSELL, W. M. S.; BURCH, R. L. **The principles of humane experimental technique**. [s.l.] Methuen, 1959.

SCHNEIDER, F. et al. **Mechanical properties of silicones for MEMS**. Journal of Micromechanics and Microengineering. **Anais**...1 jun. 2008.

SOSA-HERNÁNDEZ, J. E. et al. Organs-on-a-Chip Module: A Review from the Development and Applications Perspective. **Micromachines**, v. 9, n. 10, 22 out. 2018.

SRINIVASAN, B. et al. TEER Measurement Techniques for In Vitro Barrier Model Systems. **SLAS Technology**, v. 20, n. 2, p. 107–126, 1 abr. 2015.

STUPIN, D. D. et al. Bio-Impedance Spectroscopy: Basics and Applications. 2020.

THESES, G.; WEERASINGHE, H. C. **Electrical Characterization Of Metal-To-Insulator Transition In Iron Silicide Thin Films On Silicon Substrates**. [s.l: s.n.]. Disponível em: <https://scholarcommons.usf.edu/etd>.

THUY, T. N. T.; TSENG, T. T. C. A micro-platinumwire biosensor for fast and selective detection of alanine aminotransferase. **Sensors (Switzerland)**, v. 16, n. 6, 1 jun. 2016.

TSVIRKUN, D. et al. Microvasculature on a chip: study of the Endothelial Surface Layer and the flow structure of Red Blood Cells. **Scientific Reports**, v. 7, n. 1, 24 mar. 2017.

UNGER, M. A. et al. Monolithic microfabricated valves and pumps by multilayer soft lithography. **Science**, v. 288, n. 5463, p. 113–116, 7 abr. 2000.

VACCARI, N. et al. White light spectroscopy for T-cell culture growth monitoring: towards a real-time and sampling free device for ATMPs production. **Journal of Translational Science**, v. 7, n. 6, 2021.

VAN DER HELM, M. W. et al. Lab on a Chip Non-invasive sensing of transepithelial barrier function and tissue differentiation in organs-on-chips using impedance spectroscopy †. v. 19, p. 452, 2019.

WACOGNE, B. et al. Absorption Spectra Description for T-Cell Concentrations Determination and Simultaneous Measurements of Species during Co-Cultures. **Sensors 2022, Vol. 22, Page 9223**, v. 22, n. 23, p. 9223, 27 nov. 2022.

WANG, K. et al. Non-Invasive Detection of Early-Stage Fatty Liver Disease via an On-Skin Impedance Sensor and Attention-Based Deep Learning. **Advanced Science**, v. 11, n. 31, 21 ago. 2024.

WHITESIDES, G. M. The origins and the future of microfluidics. **Nature 2006 442:7101**, v. 442, n. 7101, p. 368–373, 26 jul. 2006.

WU, Z. et al. Potent-By-Design: Amino Acids Mimicking Porous Nanotherapeutics with Intrinsic Anticancer Targeting Properties. **Small**, v. 16, n. 34, [s.d.].

XIA, Y.; WHITESIDES, G. M. **SOFT LITHOGRAPHYAnnu. Rev. Mater. Sci**. [s.l: s.n.]. Disponível em: <www.annualreviews.org>.

YANG, N. et al. Temperature Tolerance Electric Cell-Substrate Impedance Sensing for Joint Assessment of Cell Viability and Vitality. **ACS Sensors**, v. 6, n. 10, p. 3640–3649, 22 out. 2021.

YESTE, J. et al. A compartmentalized microfluidic chip with crisscross microgrooves and electrophysiological electrodes for modeling the blood-retinal barrier. **Lab on a Chip**, v. 18, n. 1, p. 95–105, 7 jan. 2018.

ZAOUK, R.; PARK, B. Y.; MADOU, M. J. Introduction to microfabrication techniques. **Methods in molecular biology (Clifton, N.J.)**, v. 321, p. 5–15, 2006.

ZHANG, Y. S.; ZHANG, Y.-N.; ZHANG, W. Cancer-on-a-chip systems at the frontier of nanomedicine. [s.d.].

ZHU, Y. et al. Microfluidic immobilized enzyme reactors for continuous biocatalysis. **Reaction Chemistry and Engineering**, v. 5, n. 1, p. 9–32, 1 jan. 2020.